

A Range of Outcomes: The Combined Effects of Internal Variability and Anthropogenic Forcing on Regional Climate Trends over Europe

Deleted: Role

Deleted: in

Deleted: Change

Clara Deser* and Adam S. Phillips

National Center for Atmospheric Research, Boulder CO USA

EGU Nonlinear Processes in Geophysics Special Issue

“Interdisciplinary perspectives on climate sciences – highlighting past and current scientific achievements”

Submitted October 14, 2022

Revised December 27, 2022

* Corresponding author: Clara Deser cdeser@ucar.edu

20 **Abstract**

21 Disentangling the effects of internal variability and anthropogenic forcing on regional climate

22 ~~trends~~ remains a key challenge with far-reaching implications. Due to its largely unpredictable

Deleted: change

23 nature on ~~long~~ timescales, internal climate variability limits the accuracy of climate model

Deleted: longer than a decade

24 projections, introduces challenges in attributing past climate ~~trends~~, and complicates climate model

Deleted: changes

25 evaluation. Here, we highlight recent advances in climate modeling and physical understanding

26 that have led to novel insights on these key issues. In particular, we synthesize new findings from

27 ~~Earth System Model and Observationally-based Large Ensembles (LEs), along with empirical~~

Deleted: Large Ensemble simulations with

28 “dynamical adjustment” methodologies, ~~Using the new 100-member Community Earth System~~

Deleted: s,

29 ~~Model version 2 (CESM2) LE, we show that internal climate variability imparts considerable~~

Deleted: Large Ensembles

30 ~~uncertainty to past and future 50-year trends in wintertime temperature and precipitation over~~

Deleted: ,

31 ~~Europe. Quantitatively similar levels of uncertainty in internally-generated 50-year trends are~~

Deleted: and

32 ~~found for the Observational-LE. The observed thermodynamic-residual trends based on~~

Deleted: , with a focus on European climate

33 ~~“dynamical adjustment” compare well with the CESM2-LE forced response, which is dominated~~

34 ~~by thermodynamic processes. Combining the internal variability of trends from the Observational-~~

35 ~~LE with the observed thermodynamic-residual trend yields a purely observationally-based range~~

36 ~~of trend outcomes, and provides a powerful test of the range of simulated trends in the CESM2-~~

37 ~~LE.~~

38

39 **1. Introduction**

40 *a. Internal variability and forced climate change*

41 The climate system is highly variable in both space and time. This variability originates from

42 processes within the coupled ocean-atmosphere-cryosphere-land-biosphere system, as well as

from external influences such as solar and orbital cycles, volcanic eruptions, and anthropogenic emissions of greenhouse gases and sulfate aerosols. A primary source of internally-generated variability is the atmospheric general circulation, which produces familiar day-to-day and week-to-week weather fluctuations. The non-linear nature of atmospheric dynamics limits predictability to less than a few weeks; beyond this time scale, atmospheric motions may be considered as random stochastic processes, often termed “weather noise” (e.g., Lorenz, 1963; Leith, 1973; James and James, 1992). It is important to note that such “weather noise” imparts variability on a continuum of time scales, from sub-monthly to decadal and longer (e.g., Madden, 1975; Deser et al. 2012; Thompson et al. 2015).

Another important source of internally-generated variability is the coupling between the ocean and atmosphere. Large-scale air-sea interactions give rise to distinctive patterns (or “modes”) of variability on interannual and longer time scales, including phenomena such as “El Niño – Southern Oscillation” (ENSO; Wang et al. 2017), “Pacific Decadal Variability” (PDV; Newman et al. 2016) and “Atlantic Multi-decadal Variability” (AMV; Zhang et al. 2019). Like the atmospheric general circulation, these coupled modes are governed by non-linear dynamical processes which limit their predictability. For example, forecast skill is generally limited to 1-2 years for ENSO (Jin et al., 2008; DiNezio et al. 2017; Wu et al. 2021), 5 years for PDV (Teng and Branstator, 2010; Meehl et al., 2016; Gordon and Barnes, 2022) and 10 years for AMV (Griffies and Bryan, 1997; Trenary and DelSole, 2016; Yeager et al., 2018). Beyond these predictability time horizons, internally-generated variability can be thought of as a “roll of the dice”, introducing unavoidable uncertainty to climate model projections especially at local and regional scales (e.g., Deser et al. 2012, 2014 and 2020a).

Deleted: 20

76

77 Not only does unpredictable internal variability cause irreducible uncertainty in future climate
78 projections, it also confounds interpretation of the historical climate record. For example, internal
79 variability may partially obscure the regional climate response to external forcings including
80 industrial greenhouse gas emissions, stratospheric ozone depletion and volcanic eruptions
81 (Wallace et al., 2013; Schneider et al. 2015; Lehner et al. 2016; McGraw et al. 2016). In some
82 areas, climate trends driven by internal processes may even outweigh those due to anthropogenic
83 influences over the past 30-60 years (Deser et al., 2012, 2016 and 2017; Wallace et al., 2013; Swart
84 et al. 2015; Lehner et al. 2017). It is important to note that such internally-generated multi-decadal
85 trends need not originate from slow processes within the ocean or coupled ocean-atmosphere
86 system: indeed, random fluctuations of the atmospheric circulation independent of oceanic
87 influences have been shown to drive a large fraction of long-term precipitation and temperature
88 trends over North America and Eurasia (Deser et al. 2012; McKinnon and Deser, 2018). The co-
89 existence of internal and anthropogenic factors necessitates a probabilistic approach to detection
90 and attribution of the human contribution to extreme weather events.

91

92 The prevalence of internal climate variability also complicates model evaluation efforts, since the
93 simulated temporal sequence of (unpredictable) internal variability need not match observations
94 even if the model's physics are realistic. Further, the brevity of the instrumental record provides
95 only a limited sampling of internal variability, hindering robust model evaluation. Thus, climate
96 models may show an apparent bias with respect to observations, but this could be entirely
97 attributable to sampling issues rather than indicative of a true bias due to incorrect model physics.
98 Apparent model bias due to sampling uncertainty must be kept in mind when assessing fidelity of

Deleted: influences

Deleted: anomalous

Deleted: and climate

102 simulated modes of internal variability (e.g., Wittenberg et al. 2009; Deser et al. 2017; Capotondi
103 et al. 2020; Fasullo et al. 2021; McKenna and Maycock, 2021), transient climate sensitivity (Dong
104 et al. 2021; Andrews et al. 2022), and “signal-to-noise” properties of initial-value predictions and
105 forced responses (e.g., Scaife and Smith, 2018; Smith et al., 2020; Klavans et al. 2021). In
106 particular, even with 100 years of data, sampling uncertainty is a limiting factor for evaluating
107 ENSO properties in climate models, including its global atmospheric teleconnections and
108 associated climate impacts (Deser et al. 2017 and 2018; Capotondi et al. 2020) and forced changes
109 thereof (Stevenson et al. 2012; Maher et al. 2018; Maher et al. 2022; O’Brien and Deser, 2022).
110 This issue is particularly acute for model assessment of modes of decadal variability such as PDV
111 and AMV due to the paucity of samples in the short instrumental record (Deser and Phillips 2021;
112 Fasullo et al. 2021).

113
114 ***b. Initial-condition Large Ensemble Simulations with Earth System Models***

115 To overcome the issue of sampling uncertainty, a recent thrust in climate modeling is to run a large
116 number of simulations (30-100) with the same coupled model and the same radiative forcing
117 protocol (historical and/or future scenario) but vary the initial conditions. The initial-condition
118 variation can be accomplished by introducing a random perturbation to the atmosphere on the order
119 of the model’s numerical round-off error (e.g., 10^{-14} K in the case of atmospheric temperatures;
120 Kay et al. 2015) or it can be done by selecting a different ocean state from a long control run of
121 the coupled model, or a combination of the two (Deser et al. 2020a and Rodgers et al. 2021).
122 Regardless of the method used, the initial-condition perturbation serves to create ensemble spread
123 once the memory of the initial state is lost, typically within a month for the atmosphere and a few
124 years to a couple of decades for the ocean (Yeager et al., 2018). The ensuing ensemble spread is

Deleted: xx

126 thus solely attributable to random internal variability (e.g., the “butterfly effect” in chaos theory);
 127 see Lorenz (1963) and Tel et al. (2019). Because the temporal sequences of internal variability
 128 unfold differently in the various ensemble members once the memory of the initial conditions is
 129 lost, one can estimate the forced component at each time step (at each location) by averaging the
 130 members together, provided the ensemble size is sufficiently large. The internal component in each
 131 ensemble member is then obtained as a residual from the ensemble-mean. Note that a larger
 132 ensemble may be needed for some aspects of the forced response than others, depending on the
 133 relative magnitudes of the forced response and internal variability (Milinski et al., 2020). For
 134 example, forced changes in ocean heat content may be readily detected with just a few members
 135 (Fasullo and Nerem, 2018), while forced changes in atmospheric circulation (Deser et al., 2012)
 136 or precipitation and temperature extremes (Tebaldi et al. 2021) may require 20-30 members.
 137 Detecting forced changes in the characteristics of internal variability itself, such as its amplitude,
 138 spatial pattern and remote teleconnections, may necessitate even larger ensembles (Milinski et al.,
 139 2020; Bódai et al., 2020; Bódai et al., 2022; O’Brien and Deser, 2023).

Deleted: :

Deleted: f

Deleted:

Deleted:

Deleted:

Deleted: require a much

141 Initial-condition Large Ensembles (LEs for short) have proven enormously useful for separating
 142 internal variability and forced climate change on regional scales in models, and for providing
 143 robust sampling of models’ internal variability by pooling together all of the ensemble members
 144 (e.g., Deser et al., 2012; Kay et al., 2015; Maher et al., 2019; Deser et al. 2020a; Lehner et al.,
 145 2020). They have also been used to assess externally-forced changes in the characteristics of
 146 simulated internal variability, including extreme events for which large sample sizes are crucial
 147 (e.g., Tebaldi et al., 2021; O’Brien and Deser, 2023). Additionally, they have served as
 148 methodological testbeds for evaluating approaches to detection and attribution of anthropogenic

Deleted: 2

156 climate change in the (single) observational record (e.g., Deser et al., 2016; Barnes et al., 2019;
157 Sippel et al., 2019 and 2021; Santer et al. 2019; Bonfils et al., 2019; Wills et al., 2020). Until the
158 advent of LEs, it was problematic to identify the sources of model differences in the Coupled
159 Model Intercomparison Project (CMIP) archives due to the limited number of simulations
160 (generally < 3) for each model (i.e., structural uncertainty was confounded with uncertainty due to
161 internal variability). This concern has been largely alleviated thanks to the recent availability of
162 LEs with multiple earth system models (e.g., Deser et al. 2020a; Lehner et al., 2020).

163

164 *c. Observationally-based Large Ensemble*

165 Just as in a model LE, the sequence of internal variability in the real world could have unfolded
166 differently. That is, the observational record traces only one of many possible climate histories that
167 could have happened under the same external radiative forcing. For example, El Niño and La Niña
168 events could have occurred in a different set of years, and positive or negative regimes of PDV
169 and AMV could have taken place in different decades. This concept of alternate chronologies,
170 sometimes referred to as the “Theory of Parallel Climate Realizations” (Tel et al., 2019) or the
171 notion of “Contingency” (Gould, 1989), has major implications that call for a reframing of
172 perspective. For example, it means that a single model simulation of the historical period need not
173 match the observed record, even if the model is “perfect” in its physical representation of the real
174 world’s climate. However, the statistical characteristics of the model’s internal variability must
175 agree with those of the real world, taking into account sampling uncertainty (uncertainty due to
176 limited sampling in the short observational record). Thus, while a single ensemble member need
177 not match observations, the ensemble as a whole should encompass the instrumental data, provided

178 there are enough members to adequately span the range of possible sequences of internal variability
179 (Suarez-Gutierrez et al. 2021).

180

181 Another implication of the concept of “parallel climate realizations” is that the climate trends we
182 have experienced are not the only ones that could have occurred under the same radiative forcing
183 conditions. In analogy with a model LE, the observational record is just one “member” of a larger
184 set of possible “members”, each with a different (and largely unpredictable) chronology of internal
185 variability. Although one cannot replay the “tape of history”, one can construct an “Observational
186 LE” by generating alternate synthetic sequences of internal variability from the instrumental data.
187 Conceptually, this involves removing an estimate of the forced component from the data and then
188 randomizing the residual (internal) variability in time. Importantly, the randomization procedure
189 must be done in a way that preserves the statistical properties of the observed variability including
190 its variance, temporal autocorrelation, and spatial patterns. The resulting synthetic sequences of
191 internal variability derived from the observational record can then be added back to the time-
192 evolving forced response obtained from a climate model LE.

193

194 The development of statistically-based Observational LEs is just beginning, with recent efforts
195 targeting surface climate fields (McKinnon et al., 2017; McKinnon and Deser, 2018 and 2021) and
196 carbon dioxide fluxes across the air-sea interface (Olivarez et al. 2022). Here, we focus on the
197 work of McKinnon and Deser (2018 and 2021) who constructed an Observational LE for global
198 sea level pressure (SLP) and terrestrial precipitation and temperature based on ~100 years of
199 monthly gridded instrumental data. To test the skill of their method, they applied it independently
200 to each member of a climate model LE and then compared the results to the “true” statistical

Deleted: are not unique

Deleted:

203 properties of the model’s internal variability based on the full set of ensemble members. According
204 to this test, their approach was found to be accurate to within 10-20% at most locations. They then
205 constructed a large (1000 member) ensemble of plausible “parallel worlds” of what the
206 observational record might have looked like had a different sequence of internal variability
207 unfolded by chance. Their Observational LE has been used for many applications, including
208 evaluation of internal variability in climate model LEs, assessment of uncertainty in observed 50-
209 year climate trends, and quantification of extreme precipitation risk over the Upper Colorado River
210 basin, a critical water resource for the western US (McKinnon and Deser 2018 and 2021).

211

212 *d. Dynamical Adjustment*

213 Determining the forced contribution to observed changes in climate remains an ongoing challenge.
214 Most “Detection and Attribution” methods rely on climate models to provide a set of spatial and
215 temporal “fingerprints” of forced climate change that are distinct from patterns of internal
216 variability (Hegerl et al. 2007; Santer et al. 2019; Sippel et al. 2019). These model-based
217 “fingerprints” are then used to assess the proportion of observed climate change that is due to
218 external forcing. However, model shortcomings may limit the accuracy of such methods. Thus, it
219 is also desirable to develop complementary approaches to attribution that do not rely on climate
220 model information. Two such methods, Linear Inverse Modeling (Newman, 2007) and Low-
221 Frequency Pattern Analysis (Wills et al. 2020), leverage the assumption that forced climate change
222 evolves slowly compared to the time scales of internal variability. However, decadal shifts in
223 regional anthropogenic aerosol emissions (Deser et al. 2020b; Persad et al. 2018), in addition to
224 decadal changes in solar and volcanic activity and the rate of greenhouse gas rise, present
225 challenges to this assumption and may complicate interpretation of the results.

Deleted: during the industrial era

Deleted: (Deser et al. 2020; Persad et al. 2018)

228

229 A complementary, physically-based approach to isolating the externally-forced response in
230 observations without reliance on climate model information is the technique of “Dynamical
231 Adjustment”. This method aims to remove the influence of atmospheric circulation variability
232 from ~~observed temperature and precipitation data~~, thereby revealing the thermodynamically-
233 induced component of observed climate change (Wallace et al. 2013; Smoliak et al. 2015; Deser
234 et al. 2016; Guo et al. 2019). According to the current generation of coupled climate models, the
235 forced component of extra-tropical atmospheric circulation changes is small relative to internal
236 variability (Deser et al. 2012; Shepherd, 2014). If models are correct in this regard, then dynamical
237 adjustment can be used to parse the relative contributions of internal dynamics and forced
238 thermodynamics to observed climate changes at middle and high latitudes (Wallace et al. 2013;
239 Deser et al. 2016). A variety of dynamical adjustment algorithms have been developed and tested
240 within the framework of a model LE (Deser et al., 2016; Lehner et al., 2017 and 2018; Smoliak
241 et al., 2015; Guo et al. 2019; Merrifield et al., 2017; Terray 2021; Sippel et al. 2019). These
242 protocols are all based on statistical associations between patterns of SLP and ~~temperature or~~
243 ~~precipitation~~ deduced from long observational records. Generally, the data are high-pass filtered
244 or detrended so as to avoid aliasing any potential forced component onto the statistical
245 relationships. These procedures generally work best for large-amplitude SLP anomaly patterns,
246 and are more effective for temperature than precipitation due to higher levels of noise in the latter
247 (Guo et al. 2019).

248

249 2. Data and Methods

Deleted: surface climate anomalies

Deleted: surface climate anomalies

Deleted:

253 We make use of a state-of-the-art 100-member LE conducted with the National Center for
254 Atmospheric Research (NCAR) Community Earth System Model version 2 (CESM2), described
255 in Rodgers et al. (2021). This publicly-available LE resource is unprecedented for its combination
256 of large ensemble size, high spatial resolution (approximately 1° in both latitude and longitude),
257 and length of simulation (1850-2100). Each ensemble member is driven by the same radiative
258 forcing scenario (historical from 1850-2014, and SSP3-7.0 from 2015-2100), but begins from a
259 different state on 1 January 1850, taken from a long pre-industrial control simulation. We analyze
260 linear trends in air temperature, precipitation and sea level pressure over the past 50 years (1972-
261 2021) and projected for the next 50 years (2022-2071). It should be noted that memory of the
262 initial state is negligible by the middle of the 20th century for the quantities we analyze; thus,
263 diversity in trends amongst the individual ensemble members is solely due to different random
264 samples of internal variability, which are superimposed upon a common forced response.

265

266 For consistency with the 100-member CESM2 LE, we make use of the first 100 members of the
267 Observational LE (OBS LE) constructed by McKinnon and Deser (2018) to illustrate the diversity
268 of past 50-year trends consistent with the statistical spatio-temporal properties of internal
269 variability in the observational record. For the purpose of comparing directly to the CESM2 LE,
270 we have added the model's forced trend to the internal trend of each OBS LE member. The OBS
271 LE is based on the Berkeley Earth Surface Temperature (BEST) dataset (Rohde et al. 2013), the
272 Global Precipitation Climatology Centre (GPCC) dataset (Schneider et al. 2008), and the
273 Twentieth Century Reanalysis version 2c (20CR) sea level pressure (SLP) dataset (Compo et al.
274 2011).

275

276 We apply the dynamical adjustment methodology of Deser et al. (2016) based on SLP “constructed
277 circulation analogues” to monthly temperature and precipitation during 1900-2021, using the same
278 observational data sets as in the OBS LE. The reader is referred to Deser et al. (2016) for details
279 of the methodology, and to Lehner et al. (2017 and 2018), Guo et al. (2019) and Terray (2021) for
280 additional applications.

281

282 For each ensemble member of the CESM2 and OBS LEs, we form monthly anomalies by
283 subtracting the long-term means for each month individually, and then form seasonal averages
284 (December-February) of the monthly anomalies. We compute 50-year trends of the wintertime
285 anomalies using linear least-squares regression analysis. All results shown in this study are
286 original findings.

287

288 **3. European climate trends**

289 We begin by illustrating the diversity of winter temperature and precipitation trends over Europe
290 during the past 50 years (1972-2021) in the CESM2 and OBS LEs (Sections 3a and b), and
291 projected for the next 50 years (2022-2071) in the CESM2 LE (Section 3c). We then provide a
292 more quantitative view of the relative contributions of forced climate change and internal
293 variability to past and future climate trends using a variety of signal-to-noise metrics, with
294 comparison between the CESM2 and OBS LEs (Section 3d). We summarize the CESM2 LE
295 results by showing the “expected range” of trend outcomes in Section 3e. Finally, we apply the
296 technique of “dynamical adjustment” to estimate the forced component of observed temperature
297 trends (Section 3f), and then use this estimate in conjunction with the OBS LE to produce a purely

298 observational estimate of the plausible range of temperature trend outcomes over the past 60 years
299 (Section 3g).

300

301 ***a. Past trends (1972-2021) in the CESM2 LE***

302 The CESM2 model simulates a wide range of wintertime temperature trend patterns for the past
303 50 years due to the combined effects of internal variability and forced response, as illustrated by
304 the first 28 members of the LE (Fig. 1). Recall that the only reason that these trend maps are not
305 identical is because of random differences in internal variability between the members. While
306 moderate warming is seen over most of the European continent in the majority of cases, as
307 expected, some members show regions of considerably greater temperature increase (in excess of
308 1°C per decade for example members 1, 10 and 18), while others exhibit weak cooling in some
309 locations (for example, members 17, 23 and 26; Fig. 1). The relative contributions of internal
310 variability and forced response can be readily discerned by comparing the individual member
311 trends with the ensemble-mean trend (see “EM” panel in Fig. 1). The observed trend (“OBS”
312 panel in Fig. 1) bears a close resemblance to the model’s forced trend in both amplitude and spatial
313 pattern. This correspondence may be coincidental, as individual members of the CESM2 LE also
314 resemble the forced response (for example, members 6 and 21), or it may suggest that the model
315 overestimates the amplitude of internally-generated 50-year trends relative to forced trends. The
316 OBS LE results shown below will shed some light on these two possibilities.

CESM2 large ensemble: Temperature trends 1972-2021

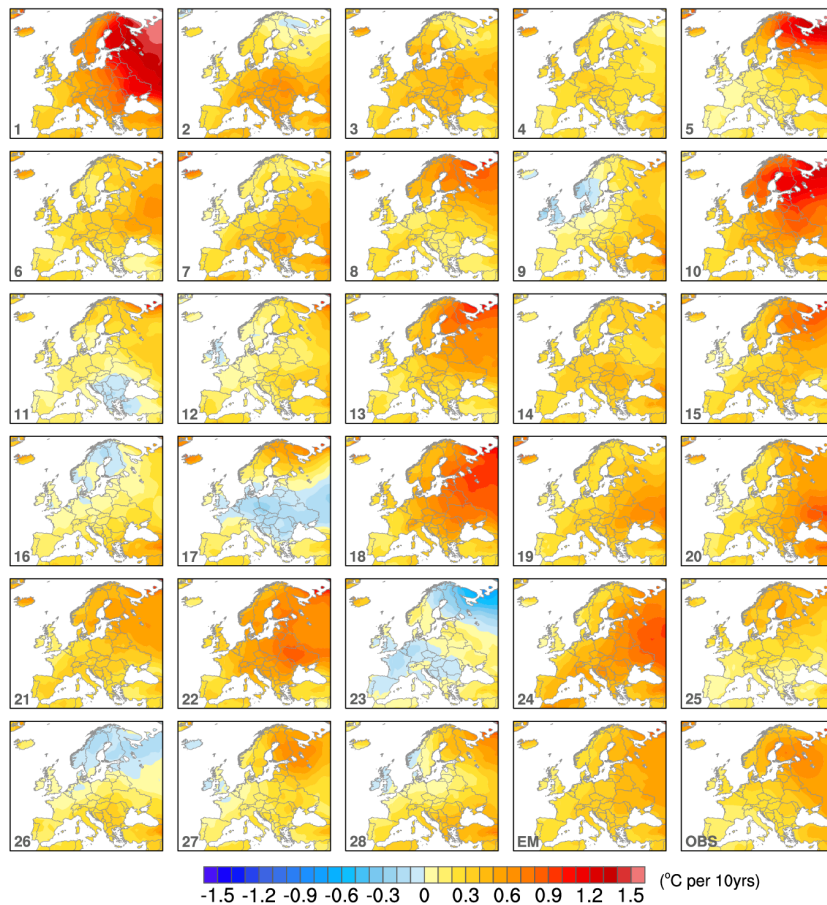
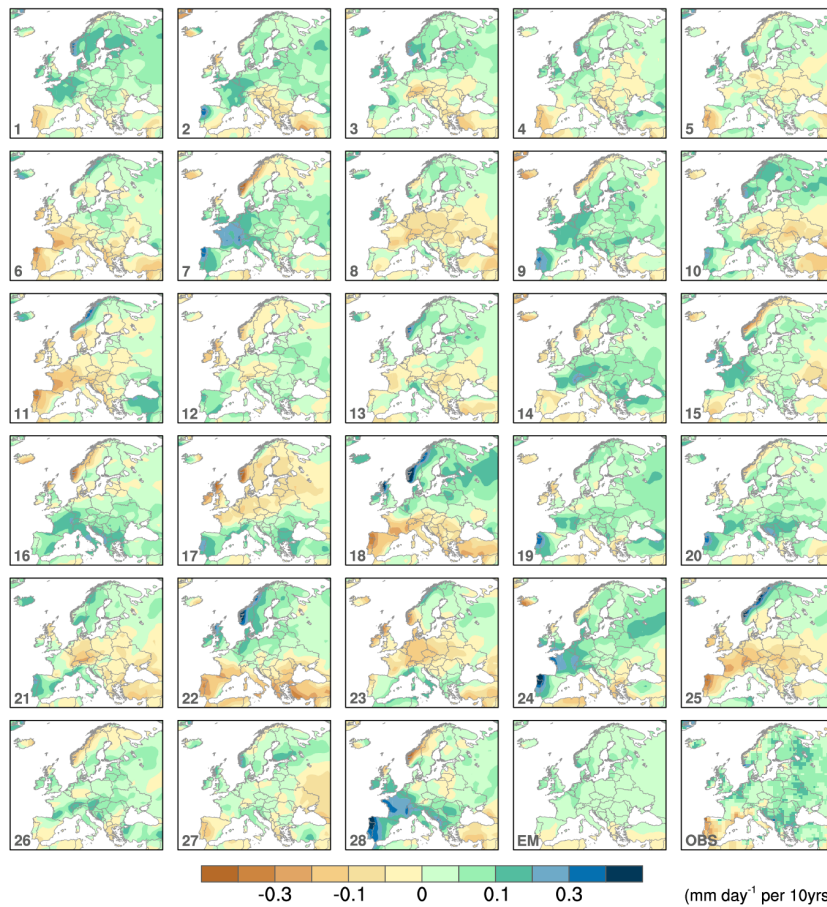


Figure 1. Winter air temperature trends ($^{\circ}\text{C}$ per decade) for the period 1972-2021 as simulated by the first 28 members of the CESM2 Large Ensemble (number in the lower left of each panel denotes the ensemble member) and the 100-member ensemble-mean (panel labeled “EM”). Observed trends are shown in the lower right (panel labeled “OBS”).

CESM2 large ensemble: Precipitation trends 1972-2021



323

324 **Figure 2.** As in Fig. 1 but for precipitation (mm d-1 per decade).

325

326 Like temperature, precipitation trends also vary considerably across ensemble members (Fig. 2).

327 While the ensemble-mean trend shows modest increases in precipitation throughout Europe

328 (except for the southernmost fringes), internal variability can evidently overwhelm the forced

329 response in individual simulations. For example, some members show drying over large parts of

330 the continent, while others depict enhanced wetting in the same regions (compare, for example,
331 members 22 and 28, which show nearly opposite patterns). Observed precipitation trends are
332 generally positive, except over Spain, Portugal, southern France and other parts of the western
333 Mediterranean (Fig. 2). The observed precipitation increases, while of the same sign as the
334 model's forced response, are approximately twice as large in many areas. Again, the interpretation
335 of the observed trends is ambiguous, since there are individual members that resemble
336 observations (for example, member 1).

337

338 ***b. Past trends (1972-2021) in the OBS LE***

339 The individual members of the OBS LE show a qualitatively similar diversity of 50-year
340 temperature trends as the CESM2 LE (Fig. 3). Like CESM2, some members show weak cooling
341 in some areas while others show widespread moderate or strong warming. This suggests that the
342 resemblance between the observed trend and the model's forced response may be purely
343 coincidental. Precipitation trends in the OBS LE also display large contrasts between members,
344 similar to CESM2 (Fig. 4). For example, nearly opposite patterns are found between members 6
345 and 11 (or 8 and 9). Trend amplitudes also vary considerably across the OBS LE, with larger
346 magnitudes in some members (for example, members 3 and 20) compared to others (e.g., members
347 21 and 13). While no single member of the 28 OBS LE samples shown matches the model's forced
348 trend, member 21 with its relatively muted trends comes close.

Observational large ensemble: Temperature trends 1972-2021

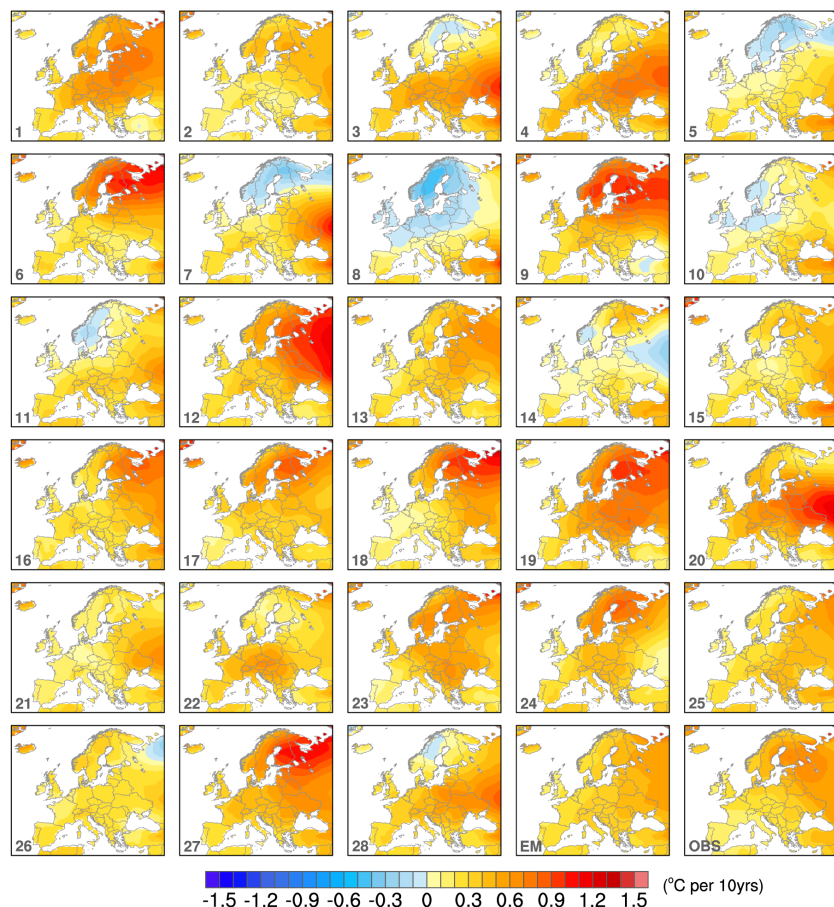


Figure 3. As in Fig. 1, but for the Observational Large Ensemble of McKinnon and Deser (2018) with the ensemble-mean from the 100-member CESM2 Large Ensemble. See text for details.

Observational large ensemble: Precipitation trends 1972-2021

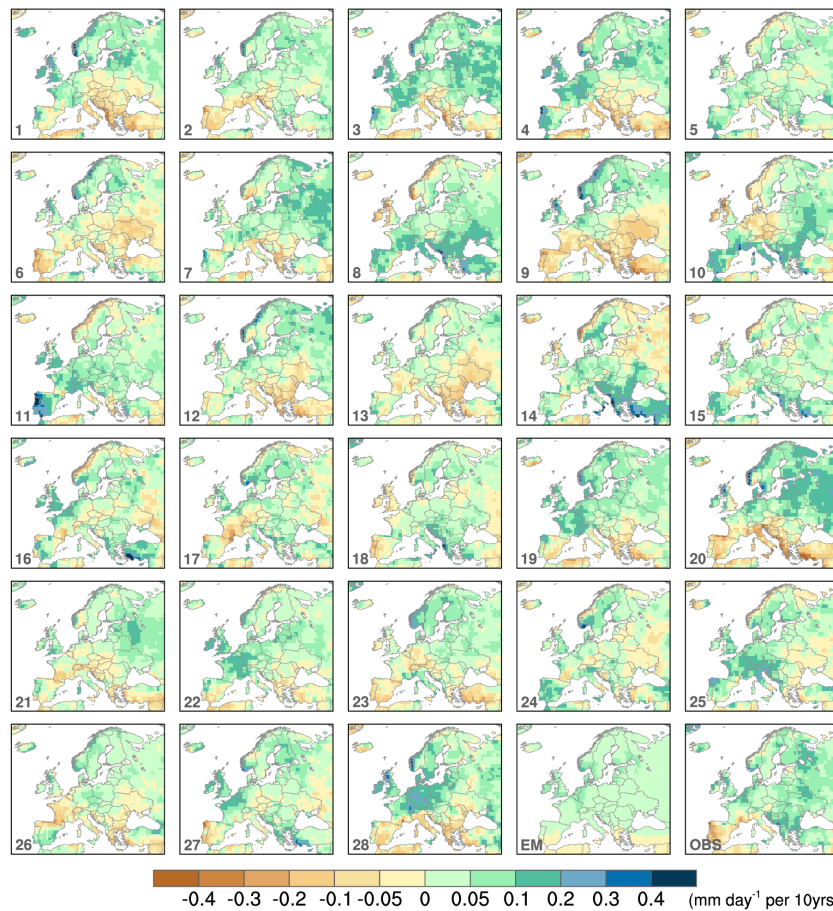


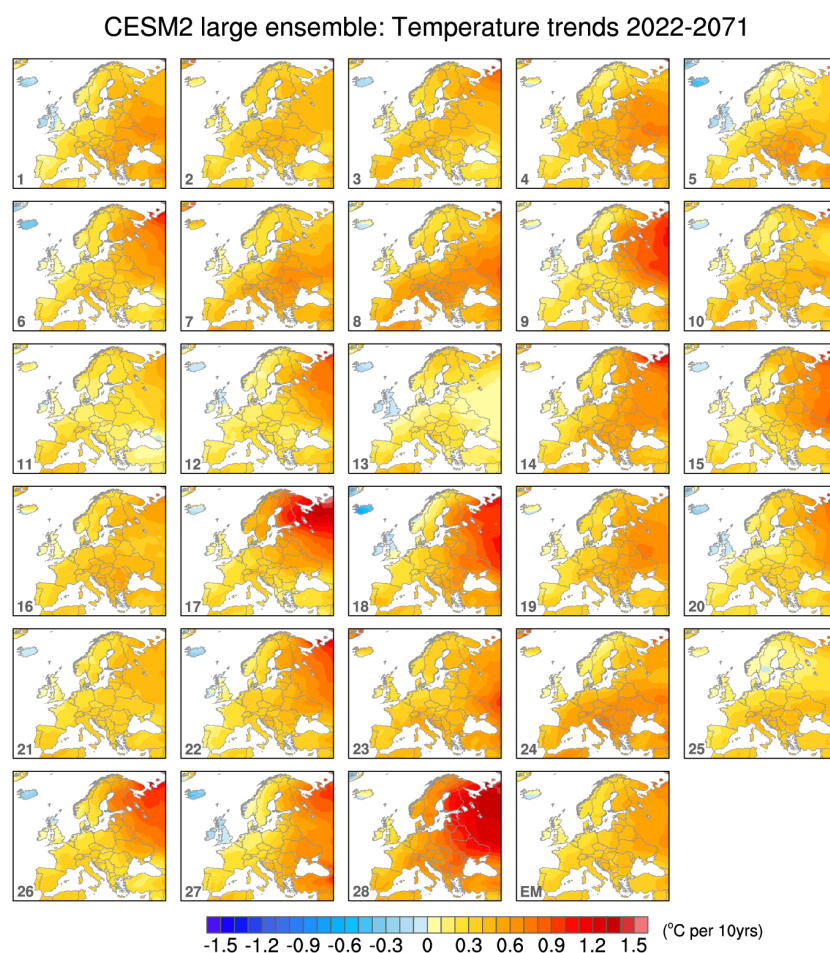
Figure 4. As in Fig. 2, but for the Observational Large Ensemble of McKinnon and Deser (2018) with the ensemble-mean from the 100-member CESM2 Large Ensemble. See text for details.

357 *c. Future Trends (2022-2071) in the CESM2 LE*

358 As expected, temperature trends projected for the next 50 years show larger amplitudes than those
359 for the past 50 years in the CESM2 LE (Fig. 5). This is due to the fact that the forced (ensemble-
360 mean) component of warming increases as greenhouse gas emissions accelerate. In most regions,
361 the forced warming trend increases by approximately 0.2°C per decade in the future compared to
362 the past. Notable exceptions are Iceland and the British Isles, which show less warming in the
363 future due to a circulation-induced forced cooling trend (see Section 3e). Despite a larger forced
364 component, temperature trends projected for the next 50 years still show a wide range of
365 amplitudes across individual members of the CESM2 LE. For example, member 13 is striking for
366 its muted warming (generally < 0.5°C per decade) across Europe (and absolute cooling over the
367 UK and Iceland), while member 28 shows highly amplified warming, with values exceeding 1.3
368 °C per decade over western Russia.

369
370 Forced trends in precipitation are projected to amplify over the next 50 years, with greater wetting
371 over northern Europe and drying over southern Europe and the Mediterranean (Fig. 6). In addition,
372 the region with a forced drying trend is projected to expand northward into Spain, Italy and the
373 Balkan Republics. While the forced pattern of future drying in the south and wetting in the north
374 is generally evident in most of the simulations shown, there are notable differences in amplitude
375 across the members. For example, member 28 shows precipitation trends in excess of 0.1 mm d⁻¹
376 per decade over most of northern Europe, while member 11 shows positive precipitation trends of
377 less than half this amount. Members 27 and 28 illustrate that the mid-section of the European
378 continent may get wetter or drier depending on the unpredictable sequence of internal variability

379 that unfolds. Thus, internal variability can still make a sizeable contribution to the projected
 380 patterns and amplitudes of winter precipitation trends over the next 50 years.
 381



382

383 **Figure 5.** As in Fig. 1, but for the period 2022-2071.

384

385

CESM2 large ensemble: Precipitation trends 2022-2071

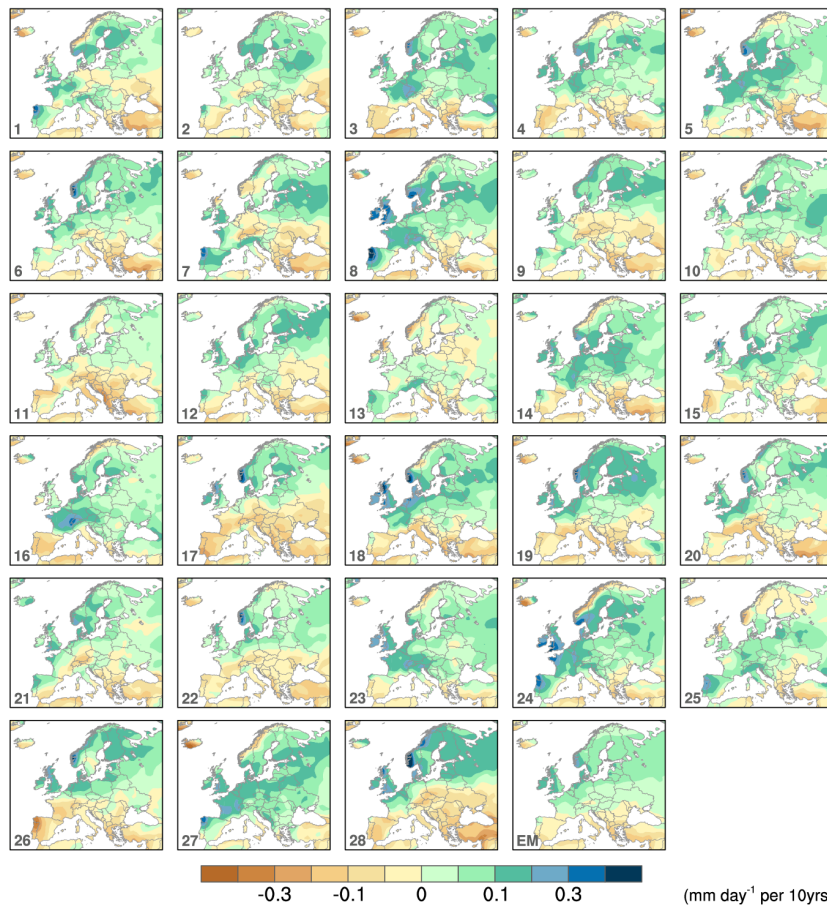


Figure 6. As in Fig. 2, but for the period 2022-2071.

389 *d. Signal-to-noise metrics and model evaluation.*

390 In the previous section, we conveyed a qualitative impression of the possible range of 50-year
391 trends due to the superposition of internal variability and forced climate change in the CESM2 and
392 OBS LEs. Here, we provide a more quantitative view, beginning with a comparison of the standard
393 deviation (σ) of trends over the period 1972-2021 computed across the ensemble members of each
394 LE. In the CESM2 LE, the ensemble σ of temperature trends increases from southwest to
395 northeast, with minimum values (0.05-0.10 K per decade) over Spain and northern Africa, and
396 maximum values (0.30-0.35 0.5°C per decade) over northwestern Russia (Fig. 7a). A similar
397 pattern is found in OBS LE, with some regional differences in amplitude (Fig. 7b). In particular,
398 the ensemble σ values are significantly smaller (20-40%) over Scandinavia, Germany and Poland,
399 and significantly larger (20-40%) in areas near the Mediterranean and Black Seas, in the OBS LE
400 compared to the CESM2 LE (Fig. 7c). For precipitation trends, the two LEs show similar patterns
401 of ensemble σ , with largest amplitudes generally along the west coasts (0.10 - 0.25 mm d⁻¹ per
402 decade) and over southwestern Europe (values 0.05 – 0.10 mm d⁻¹ per decade: Figs. 7d and e).
403 However, CESM2 LE significantly underestimates the OBS LE by more than 40% along the
404 Mediterranean and Black Seas and parts of Russia, and significantly overestimates the OBS LE by
405 20-40% in many areas of western Europe (Fig. 7f).

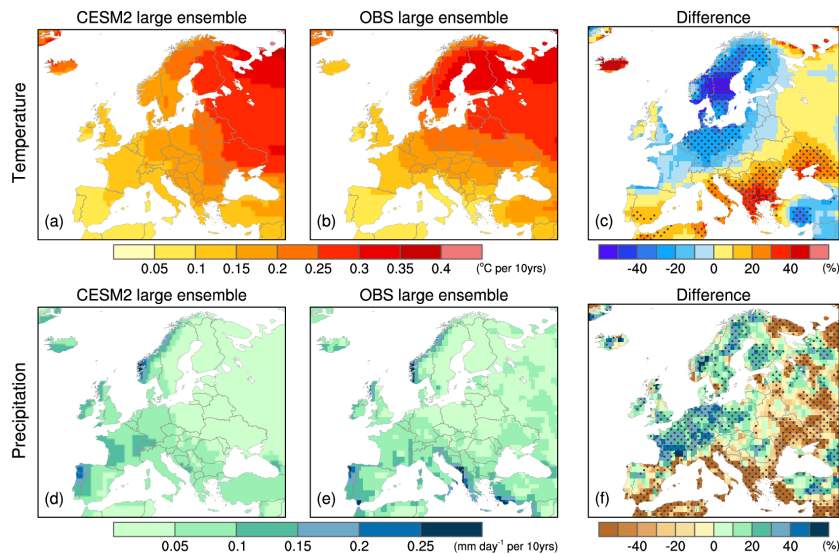


Figure 7. Standard deviation of 50-year trends (1972-2021) across 100 members of the CESM2 Large Ensemble (a,d) and 100 members of the Observational Large Ensemble (b,e), and their difference (c,f) for winter air temperature (top; °C per decade) and precipitation (bottom; mm d⁻¹ per decade). Stippling in panels c and f indicates that the differences are statistically significant at the 95% confidence level according to an f-test.

Next, we assess the relative magnitude of the forced and internal components of trends by computing a “signal-to-noise” ratio defined as the CESM2 ensemble-mean trend divided by the σ of trends across the 100 members of each LE. This “signal-to-noise” ratio provides a metric of the likelihood that the ensemble-mean (e.g., forced) trend might be overwhelmed by the internally-generated trend in any given ensemble member (and by extension, the real world). Assuming that the 100-member set of 50-year trends follows a normal distribution (not shown, but see related results in Deser et al. 2012; Thompson et al. 2015; Deser et al. 2020a), a signal-to-noise ratio greater than one (two) indicates that the magnitude of the ensemble-mean (forced) trend is larger than (more than twice as large as) that of a typical (e.g., one standard deviation) internal trend, and

Deleted: ly

Formatted: Font: Not Italic

Formatted: Font: Not Italic

Formatted: Font: Not Italic

Deleted: indicates whether the forced trend can be readily detected in any single ensemble member

Deleted: , or whether internal variability dominates

Formatted: Font: Not Italic

Deleted: For

Formatted: Font: Not Bold

Formatted: Font: Not Italic

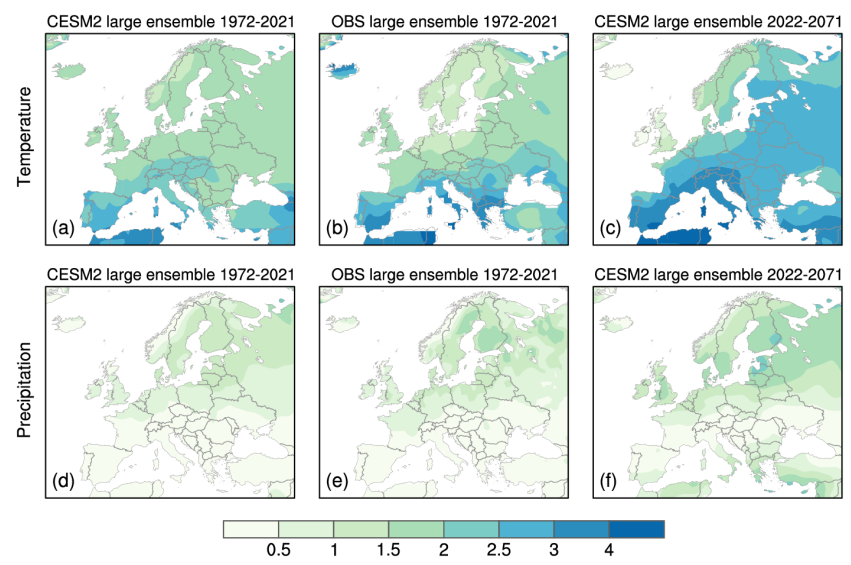
427 a signal-to-noise ratio less than one indicates that the amplitude of a typical internal trend exceeds
 428 the magnitude of the forced trend. In the CESM2 LE, the signal-to-noise of forced temperature
 429 trends over the past 50 years generally ranges from 1.5 - 2 over central and northern Europe, and
 430 from 2-3 over southern Europe (Fig. 8a). Forced precipitation trends over the past 50 years exhibit
 431 much lower signal-to-noise ratios than temperature, with values generally < 1 and nearly always
 432 < 1.5 (Fig. 8d).

Formatted: Font: Not Italic

Formatted: Font: Not Italic

Deleted: significantly different from zero at the 95% confidence level: that is, there is less than a 5% chance that the ensemble-mean trend could have been a result of random internal variability.

Formatted: Font: Not Italic



433

434 **Figure 8.** Signal-to-noise of forced trends in winter (top) air temperature and (bottom)
 435 precipitation based on the 100-member CESM2 Large Ensemble during 1972-2021 (a,d), the
 436 Observational Large Ensemble during 1972-2021 (b,e), and the CESM2 Large Ensemble during
 437 2022-2071 (c,f). See text for details.
 438

439 How much do model biases in ensemble σ shown previously affect the signal-to-noise of the
 440 model's forced trends? We address this question by using the OBS LE σ values in place of the
 441 model's σ values in the signal-to-noise calculation (note that the "signal" in the two LEs is identical

Formatted: Font: Not Bold, Not Italic

446 [by construction](#)). This substitution results in an enhancement of signal-to-noise of past forced
 447 temperature trends over southern Europe and a reduction in signal-to-noise over Scandinavia,
 448 Germany and Poland, with a net increase from 38% to 60% in the area with values > 2 (Fig. 8b).
 449 The impact of model biases in ensemble trend σ is much less pronounced for precipitation than
 450 temperature, with signal-to-noise values in all locations remaining below 2 (Fig. 8e).
 451
 452 As expected, signal-to-noise values are higher for forced trends in the future than in the past.
 453 Ninety-seven percent of the area of the continent (excluding Iceland and Greenland) shows a
 454 signal-to-noise value > 2 for forced temperature trends during 2022-2071 (Fig. 8c), compared with
 455 38% for trends during 1972-2021. Forced precipitation trends in the future remain uncertain, with
 456 only 2% of the land area showing a signal-to-noise value > 2 (Fig. 8f).
 457
 458 Another way to view the relative impacts of internal variability and external forcing on trends is
 459 by computing the fraction of ensemble members at each location that show a positive trend (e.g.,
 460 warming or wetting). This metric conveys the likelihood of having a positive (or negative) trend
 461 in any single ensemble member, which is analogous to the single “realization” of the real world.
 462 At nearly all locations, more than 95% of ensemble members in the CESM2 LE show warming in
 463 both the past and future periods, with slightly lower percentages (85-95%) over western
 464 Scandinavia and parts of Great Britain (and < 75% over Ireland, Scotland and Iceland in the
 465 future); (Figs. 9a and c). Similar percentages are obtained when the internal component of past
 466 temperature trends in the OBS LE is used in place of the model’s internal trends, with some
 467 reduction (75-95%) over Scandinavia, northern Russia, Germany and Poland (Fig. 9b).

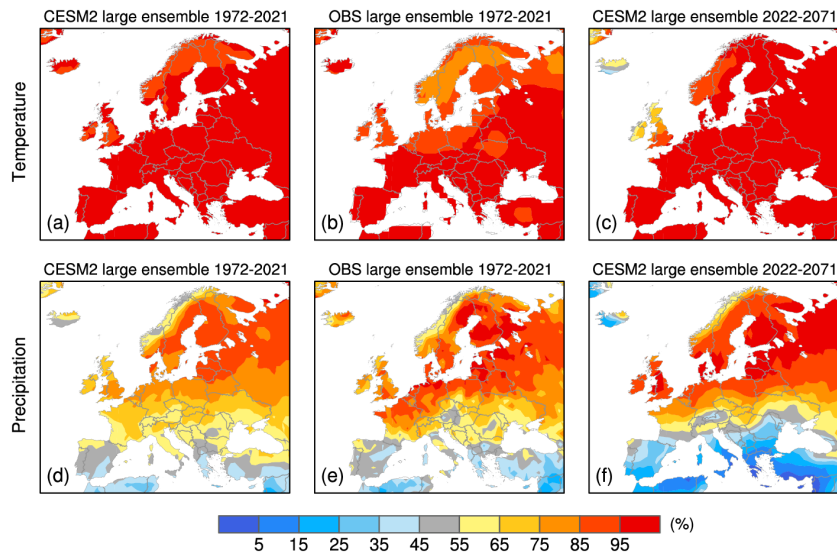


Figure 9. The percentage of ensemble members with a positive trend in winter (top) air temperature and (bottom) precipitation trends based on (a,d) the 100-member CESM2 Large Ensemble during 1972-2021, (b,e) the 100-member Observational Large Ensemble during 1972-2021, and (c,f) the 100-member CESM2 Large Ensemble during 2022-2071.

The sign of the trend in any given ensemble member is more uncertain for precipitation than for temperature. The highest chances (> 85%) of a positive precipitation trend are found over the northernmost third of the continent excluding Norway, both in the past and future (Figs. 9d and f). Similarly high chances of a negative precipitation trend (equivalent to < 15% of a positive trend) occur in areas near the Mediterranean Sea, but only in the future. The central portion of the continent shows roughly equal chances of having a positive or negative trend, both in the past and future. The area with a > 85% chance of a positive precipitation trend in the past 50 years expands southward into northern France, Germany and areas bordering the Baltic Sea when internal variability is derived from the OBS LE compared to the CESM2 LE (Fig. 9e).

484 Taken together, the results shown in Fig. 9 indicate that warming is virtually guaranteed at nearly
485 all locations, both in the past 50 years and the next 50 years, according to the CESM2 LE.
486 However, the sign of the precipitation trend (past and future) is robust only over the northern tier
487 of the continent, and only in the future over the Mediterranean region. The model results for past
488 trends are found to be generally credible as measured against the OBS LE, with some
489 overestimation in north-central Europe.

490

491 *e. Range of outcomes and the role of the atmospheric circulation*

492 As the saying goes, “climate is what we expect, weather is what we get”. This adage is also
493 applicable to climate change, where “human-induced climate change is what we expect, internal
494 variability plus human-induced climate change is what we get” (Deser 2020). Here, we illustrate
495 “what we expect” and the range of “what we get” for past and future 50-year trends in the CESM2
496 LE, using the ensemble-mean for “what we expect” and two contrasting ensemble members for
497 the range of “what we get”. We select the contrasting members from the bottom and top 5th
498 percentiles of the distribution of 100-member trends averaged over the European continent for
499 each period separately. This selection criterion is somewhat arbitrary and does not necessarily
500 capture the wide range of trend amplitudes that may occur at a single location or sub-region, nor
501 does it portray the full range of spatial patterns that occur within the ensemble.

502

503 There is a large range in temperature trend outcomes (“what we get”) for both the past 50 years
504 and the next 50 years as depicted by the “warm” and “cool” end-members (Fig. 10). For past
505 trends, the “warm” end-member shows temperature increases of 0.9-1.1 °C per decade over the
506 eastern portion of the continent (Fig. 10b), while the “cool” end-member displays muted warming

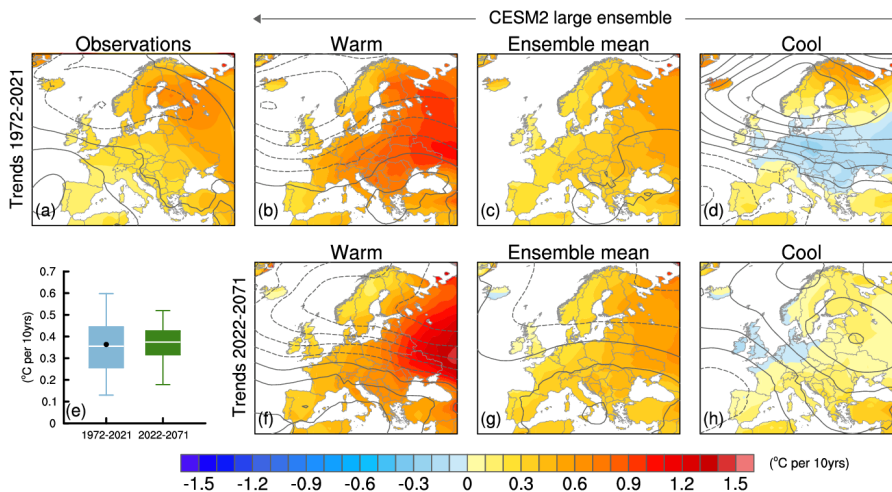


Figure 10. A Range of Outcomes. Trends in winter air temperature (color shading; °C per decade) and sea-level pressure (SLP) (contours; contour interval of 0.25 hPa per decade, negative values dashed) for the period (top) 1972-2021 and (bottom) 2022-2071. Panel (a) shows observed trends (1972-2021) and remaining panels show simulated trends from the 100-member CESM2 Large Ensemble: (c,g) ensemble-mean; (b,f) “warm” end-member; (d,h): “cool” end-member. See text for details. *Note that panels (a) and (c) are identical to the “OBS” and “EM” panels in Fig. 1, respectively.* Panel (e): Distribution of European-average trends for 1972-2021 (blue) and 2022-2071 (green) from the CESM2 Large Ensemble (box outlines 25th-to-75th percentile range, whiskers mark the 5th-to-95th percentile range, the horizontal white line denotes the median value, and the black circle marks the observed value).

(< 0.3 °C per decade) and even slight cooling through the midsection of the continent (Fig. 10d).

Clearly, the forced trend (“what we expect”), which depicts moderate warming (0.2-0.6°C per decade) across the continent does not tell the whole story (Fig. 10c). Analogous results are found for trends projected over the next 50 years: the “warm” member shows temperature increases of 1.0-1.5 °C per decade over west-central Russia (Fig. 10f) while the “cool” member depicts <0.2°C per decade warming over most of the continent (Fig. 10h), in marked contrast to the forced trend which ranges from 0.3-0.6°C per decade (Fig. 10g). As discussed previously, the observed temperature trend map resembles the model’s ensemble-mean, but this could be by chance (Fig.

527 10a). In terms of European averages, the observed trend (0.36 °C per decade) is nearly coincident
528 with the median value of the model's trend distribution, which has a 5th-to-95th percentile range of
529 0.13-0.60 °C per decade for past 50-year trends (Fig. 10e). Curiously, the model's median trend
530 value for Europe as a whole increases only slightly in the future compared to the past, while the
531 5th-to-95th ~~and 25th-to-75th~~ percentile ranges narrow (Fig. 10e). Further work is needed to
532 understand why this is the case.

Deleted: s

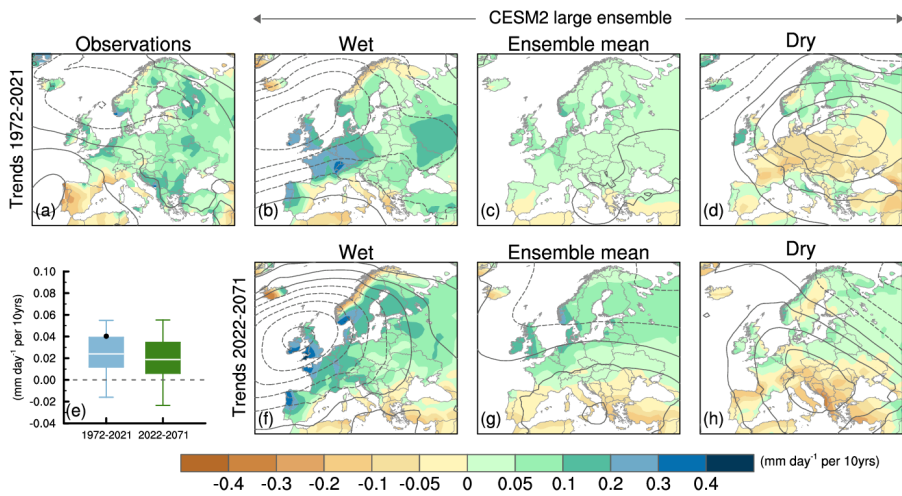
Deleted: slightly

533

534 As mentioned in Section 1d, previous work has shown that internal variability of the large-scale
535 atmospheric circulation causes much of the member-to-member differences in temperature trends
536 in model LEs. Here, we provide a qualitative indication of the circulation influence by
537 superimposing SLP trends upon the maps in Fig. 10. In the case of past trends, the “warm” member
538 shows a positive North Atlantic Oscillation (NAO)-like pattern (Hurrell et al. 2003), with negative
539 SLP trends centered near Iceland and positive SLP trends centered over the Mediterranean (Fig.
540 10b). This SLP pattern is indicative of stronger westerly/southwesterly flow, which brings
541 relatively warm maritime air over the continent. The “cool” member shows a largely opposite
542 flow configuration (albeit with longitudinal shifts in the SLP centers-of-action), which advects
543 relatively cold air from the east over the continent (Fig. 10d). In comparison, the forced response
544 shows negligible atmospheric circulation change (Fig. 10c). Striking contrasts in circulation are
545 also found for the future period, with a large positive NAO-like trend pattern in the “warm”
546 member and a blocking continental “High” in the “cool” member (Figs. 10f and h). Future trends
547 in SLP also contain a modest forced component indicative of enhanced westerlies over the
548 continent (Fig. 10g).

549

552 The “wet” and “dry” end-members also show striking regional contrasts in both precipitation and
 553 circulation (Fig. 11). For example, for past trends, the “wet” member shows precipitation increases
 554 of 0.2-0.3 mm d⁻¹ per decade over France, southern Germany, Portugal and the UK, and
 555 precipitation declines over northern Norway and along the Mediterranean Sea (Fig. 11b). A nearly
 556 opposite pattern is found for the “dry” member (Fig. 11d). These contrasting precipitation trends
 557 can be understood in the context of the overlying atmospheric circulation changes, with wetter
 558 areas coinciding with anomalous westerly/southwesterly flow and drier areas located under
 559 blocking anticyclones. Analogous patterns are found for future trends, with pronounced increases
 560 in precipitation over western Europe associated with the low pressure trend centered over the
 561 British Isles in the “wet” member (Fig. 11f), and generally reduced precipitation in the “dry”
 562 member associated with the blocking High centered over southern Europe (Fig. 11h).



563

564 **Figure 11.** As in Fig. 10 but for precipitation (mm d⁻¹ per decade). *Note that panels (a) and (c)*
 565 *are identical to the “OBS” and “EM” panels in Fig. 2, respectively.*
 566

567

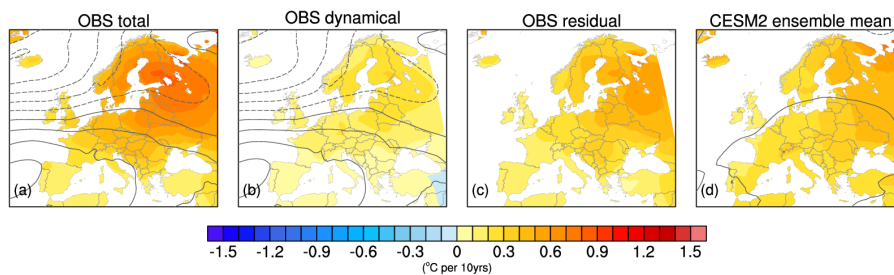
568 *f. Unmasking forced climate change in observations via “Dynamical Adjustment”*

569 The empirical method of “dynamical adjustment” introduced in Section 1d can be used to estimate
570 the circulation-induced component of observed temperature anomalies; this dynamically-induced
571 contribution can then be subtracted from the original anomaly to obtain the thermodynamically-
572 induced component as a residual. Since this method uses no information from climate models, it
573 provides an independent estimate of the thermodynamic component of observed temperature
574 trends, which can be compared with the forced response simulated by climate model LEs.

575

576 Figure 12 shows the decomposition of observed DJF temperature trends into their dynamical and
577 residual thermodynamic contributions. For this example, we have used the 60-year period 1962-
578 2021 when observed SLP trends are more than twice as large as those during 1972-2021 on a per
579 decade basis (compare SLP contours in Figs. 10a and 12a). Observed SLP trends during the past
580 60 years show a pronounced positive NAO-like pattern, with maximum negative values of -1.25
581 hPa per decade near Iceland and maximum positive values of +0.75 hPa per decade west of Spain
582 (Fig. 12a). Enhanced westerly/southwesterly flow associated with this pattern advects warm air,
583 raising surface temperatures by 0.1- 0.3°C per decade (with maximum warming over northern
584 Europe) according to the dynamical adjustment algorithm (Fig. 12b). Removing this dynamically-
585 induced component from the total trend reveals the residual thermodynamic contribution to the
586 observed warming trend (Fig. 12c). This observed thermodynamic trend is much closer in
587 amplitude (and arguably pattern) to the model’s forced response, given by the CESM2 LE
588 ensemble-mean trend (Fig. 12d), than is the total observed trend. Further, the lack of an
589 appreciable forced SLP trend in CESM2 indicates that the model’s forced temperature trend is

590 nearly all thermodynamically-driven. The level of agreement between the observed
 591 thermodynamic temperature trend and the model's forced thermodynamic trend leads to two
 592 powerful conclusions: 1) the model's forced temperature trend is realistic; and 2) removing the
 593 circulation-induced component from the observed trends can effectively reveal the influence of
 594 anthropogenic forcing. Analogous results have been found for North America (Deser et al. 2016).
 595 It may seem surprising that the model's forced temperature trend agrees so well in amplitude with
 596 the observed thermodynamic-residual trend, given that CESM2 has been characterized as a "high
 597 climate sensitivity" model (Gettelman et al., 2019). However, this characterization refers
 598 specifically to the model's equilibrium climate sensitivity (diagnosed as the model's response to
 599 an instantaneous doubling of CO₂ based on a slab-ocean configuration), and does not translate to
 600 a high transient climate sensitivity over the 1962-2021 period of record analyzed here, as
 601 evidenced by the fact that the observed global-mean temperature increase lies within the ensemble-
 602 spread of global-mean temperature trends simulated by the CESM2-LE for this time period (not
 603 shown).



606 **Figure 12.** Decomposition of (a) observed winter air temperature trends (1962-2021; °C per
 607 decade) into (b) dynamical and (c) residual thermodynamic contributions using the “dynamical
 608 adjustment” procedure of Deser et al. (2018) based on constructed circulation analogues (see text
 609 for details). Contours in (a) show observed sea-level pressure (SLP) trends (contour interval of
 610 0.25 hPa per decade, negative values dashed); contours in (b) show the observed SLP trends

611 estimated from the constructed circulation analogues; contours in (c) based on the difference
612 between (a) and (b) are near-zero and not shown. Panel (d) shows the ensemble-mean temperature
613 and SLP trends from the 100-member CESM2 Large Ensemble (note that only the zero contour
614 shows up in panel d).
615

616 Precipitation is an inherently noisier field than temperature in both time and space, making it
617 challenging to extract the forced signal via “dynamical adjustment”; indeed, only one previous
618 study has attempted dynamical adjustment of observed precipitation trends (Guo et al. 2019).
619 Keeping in mind that the estimate of the circulation-induced component of precipitation trends
620 may be less robust than for temperature, we present the results as a proof-of-concept. Observed
621 precipitation trends during 1962-2021 are mainly driven by changes in atmospheric circulation,
622 with a small thermodynamic residual component (Fig. 13). This residual component bears some
623 resemblance to the forced response in CESM2, particularly in terms of amplitude (~ 0.05 mm d⁻¹
624 per decade; Fig. 13d). Notable areas of agreement in the sign of trends include drying over most
625 of Spain, Portugal, Algeria, Turkey and Syria, and wetting over parts of northern and north-central
626 Europe; disagreement in sign is found over many central European countries (France, Germany,
627 Switzerland, Austria, Ukraine, Romania and southern Russia) where the signal-to-noise is low,
628 (Figs. 8d,e) due to a combination of low signal in the transition region between southern drying
629 and northern wetting (Fig. 11c) and high noise (Figs. 7d,e). The low signal and high noise in these
630 areas limits the accuracy of the dynamical adjustment results, where the error of the method is of
631 the same amplitude as the thermodynamic-residual trend (see Guo et al., 2019 for details).
632

Deleted: the

Deleted: much

Deleted: southern Europe

Deleted: ;

Deleted:

Deleted: shows less agreement in polarity, unsurprisingly since this region was found to have lower

Deleted: than other areas

Deleted: .

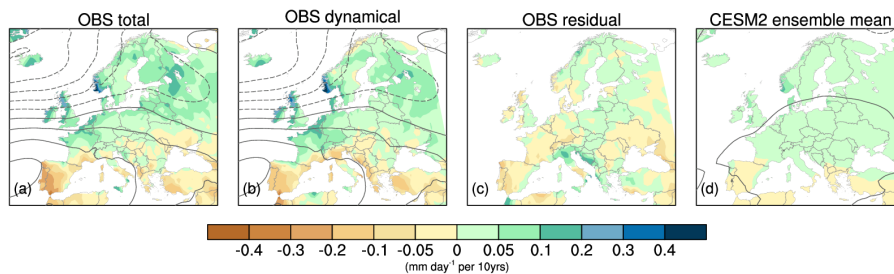


Figure 13. As in Fig. 12 but for precipitation (mm d⁻¹ per decade).

g. Toward an observationally-based “range of outcomes”

We conclude by bringing together the results of the Observational LE and “dynamical adjustment” to produce a fully observationally-based estimate of the range of past 60-year trends in temperature and precipitation. To the best of our knowledge, this is first time that these two approaches have been combined. Specifically, we add the internal component of trends from each member of the OBS LE to the thermodynamic-residual trend (the estimated observed forced response) obtained from dynamical adjustment. As before, we select two contrasting ensemble members from the tails of the distribution based on European-wide averages to illustrate the range of trend outcomes. The “warm” end-member shows pronounced temperature increases over the northern two-thirds of the continent, with maximum values in excess of 0.9 °C per decade, while the “cool” end-member warms less than 0.2 °C per decade in most areas and even cools slightly over Ukraine and neighboring countries (Figs. 14 b and d, respectively). These divergent temperature trends are associated with contrasting SLP trends, with a positive NAO-like pattern in the “warm” member a negative (and eastward-shifted) NAO pattern in the “cool” member (Figs. 14 b and d). Qualitatively, this range of trend outcomes for both temperature and SLP is remarkably similar to that obtained directly from the CESM2 LE, with some regional differences in the location of

cooling in the “cool” end-member (Figs. 14 e and g). There is no guarantee that the patterns and amplitudes of trends sampled in our selected end-members will agree between the model and observationally-based results, since there are many configurations that produce extremes in European-wide averages (not shown). That there is a strong qualitative resemblance between them is a testament to both the realism of the model’s forced response and internal variability, and the efficacy of the OBS LE and dynamical adjustment approaches.

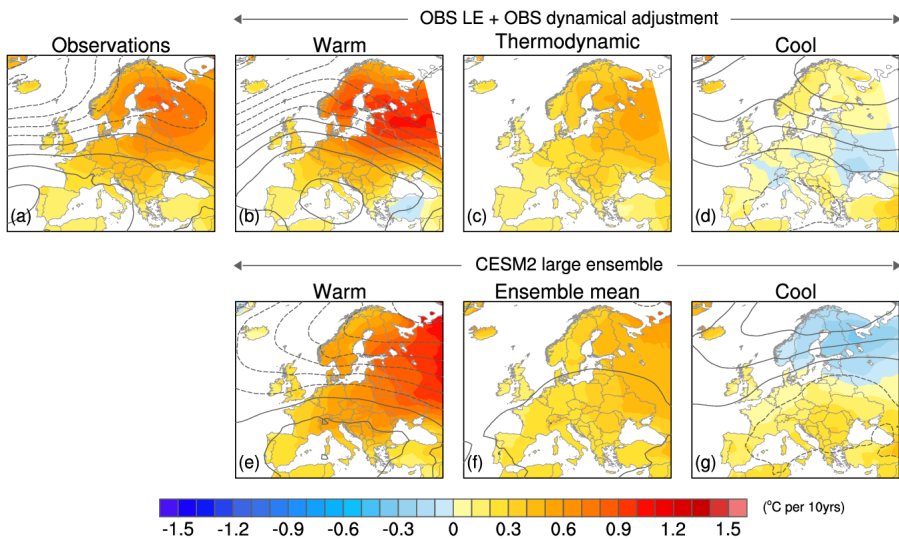
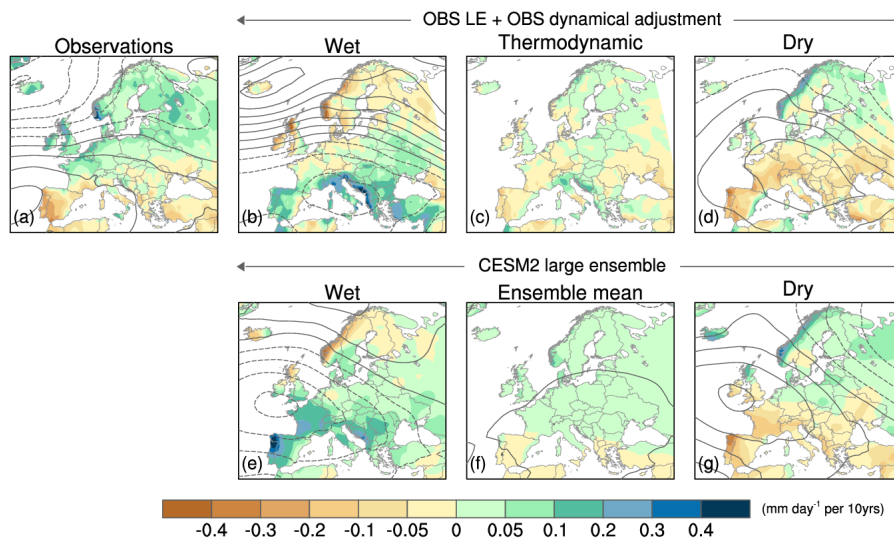


Figure 14. As in Fig. 10 but for the period 1962-2021. The top row is based on the Observational Large Ensemble combined with the residual thermodynamic component of observed trends. The bottom row is based on the 100-member CESM2 Large Ensemble. See text for details. Precipitation trends in the “wet” and “dry” end-members are also similar between the model and observationally-based results (Fig. 15). The “wet” members show widespread increases in precipitation over southern and central Europe (maximum values of 0.2-0.4 mm d⁻¹ per decade) and drying over the northern UK and parts of Scandinavia (Figs. 15 b and e). Largely opposite patterns prevail in the “dry” members (Figs. 15 d and g). The contrasting precipitation trends in

676 the “wet” and “dry” end-members are associated with opposite flow configurations, with regions
 677 of drying corresponding to high pressure and vice versa.

Deleted: ”



678
 679 **Figure 15.** As in Fig. 14 but for precipitation (mm d^{-1} per decade).
 680

681 4. Summary and open questions

682 Disentangling the effects of internal variability and anthropogenic forcing on regional climate
 683 trends remains a long-standing issue in climate sciences. Recent advances in climate modeling and
 684 physical understanding have led to new insights on this topic, and provided an improved source of
 685 information on the future risks of weather extremes associated with human-induced climate
 686 change. Here, we have highlighted new findings for European winter climate based on the
 687 following complementary tools: Earth System Model Large Ensemble simulations; an
 688 observationally-based Large Ensemble; and an empirical approach for removing the influence of

Deleted: change

Deleted: climate and

692 atmospheric circulation variability from observed ~~temperature and precipitation data, termed~~
693 ~~“dynamical adjustment”~~.

Deleted: internal

Deleted: climate anomalies

694
695 The new 100-member CESM2 Large Ensemble shows that internal climate variability imparts
696 considerable ~~uncertainty~~ to past and future 50-year trends in winter temperature and precipitation
697 over Europe. Such uncertainty is irreducible due to the lack of predictability of the simulated
698 internal variability on decadal time scales. A novel synthetic Large Ensemble constructed from the
699 statistical characteristics of internal variability in the observational record exhibits quantitatively
700 similar levels of uncertainty in past 50-year trends as the CESM2 LE, reinforcing the credibility
701 of the model’s internally-generated trends. Additionally, the results of our “dynamical adjustment”
702 procedure applied to observations shows good agreement between the observed thermodynamic-
703 residual trend component and the model’s forced thermodynamic trend, further underscoring the
704 realism of CESM2. Finally, ~~we have combined internal variability of trends from an Observational~~
705 Large Ensemble with an observational estimate of the forced trend (the thermodynamic-residual
706 component obtained from “dynamical adjustment”) to show what the observed range of past trends
707 in European temperature and precipitation could have been. Because it does not rely on climate
708 model information, this observationally-based range of trend outcomes provides a powerful test of
709 the range of simulated trends in a model Large Ensemble. ~~To the best of our knowledge, this is the~~
710 ~~first time that such a synthesis of the two purely observational methods has been undertaken.~~

Deleted: y

Deleted: for the first time,

711
712 Many outstanding questions remain regarding the relative influences of internal climate variability
713 and anthropogenic forcing on regional climate change in models and the real world. Fortunately,
714 promising new tools are being developed to help address these challenges. For example, innovative

719 machine learning methods may be able to improve upon existing techniques for constructing
 720 Observational Large Ensembles. Such methods have shown good results as statistical emulators
 721 of model-based LEs, but their application to the observational record remains to be pursued
 722 (Beusch et al. 2019). Similarly, neural network approaches to dynamical adjustment may offer
 723 increased skill compared to conventional methods (Davenport and Diffenbaugh, 2021), but have
 724 yet to be applied with the aim of separating forced and internal components of observed trends.
 725 Complementary physically-based approaches such as Linear Inverse Modeling and Low-
 726 Frequency Pattern Analysis mentioned in Section 1d also offer promise for estimating the forced
 727 response in observations without reliance on climate models and should be pursued more widely.

728

729 We have relied on the fact that the CESM2 LE (like other models of its class; see Deser et al.
 730 2020a and references therein) simulates a negligible forced atmospheric circulation trend over the
 731 past 50-60 years to interpret our observed dynamical adjustment results (i.e., we have equated the
 732 observed dynamically-induced trend with the internal component, and the observed
 733 thermodynamic-residual trend with the forced component). If the model is erroneous in this regard,
 734 then our interpretation of our decomposition of observed trends into “internal dynamical” and
 735 “forced thermodynamic” components is flawed. Recent work suggests that large-scale extra-
 736 tropical atmospheric circulation variability simulated by climate models may be less predictable
 737 on seasonal-to-decadal timescales than that in the real world, implying that models underestimate
 738 the signal-to-noise ratio of predictable components (Scaife et al. 2014; Eade et al. 2014; Scaife and
 739 Smith, 2018). But the underlying mechanisms for this underestimation, and whether this so-called
 740 “signal-to-noise paradox” found in initial-value predictability studies applies to models’
 741 atmospheric circulation response, to anthropogenic forcing, remain unknown at this time.

Deleted: Indeed, r

Deleted: climate model

Deleted: s

Deleted: particularly in terms of the large-scale extra-tropical atmospheric circulation

Deleted:

Deleted: the so-called “signal-to-noise” paradox; e.g.,

Deleted:

Deleted: e

Deleted: results from such

Deleted: s carry over

Deleted: forced

Deleted: s

Deleted: emissions

Deleted: s

Deleted: an open question

Emerging efforts to develop higher-resolution (km scale) global coupled climate models may provide the key to addressing this elusive challenge (Slingo et al. 2022).

Data and code availability statement

All data used in this study are publicly available as follows:

CESM2 Large Ensemble: <https://www.earthsystemgrid.org/dataset/ucar.cgd.cesm2le.output.html>

GPCC precipitation: <https://www.dwd.de/EN/ourservices/gpcc/gpcc.html>

BEST temperature: <http://berkeleyearth.org/data/>

and ERA5 SLP: <https://www.ecmwf.int/en/forecasts/dataset/ecmwf-reanalysis-v5>

Code used to create the Observational Large Ensemble and Dynamical Adjustment results are publicly available at:

https://github.com/karenamckinnon/observational_large_ensemble/ and

<https://github.com/terrayl/Dynamico>, respectively.

Author contributions

CD led the overall effort and wrote the manuscript. ASP performed some of the calculations and prepared the figures.

Competing interests

The contact author has declared that none of the authors has any competing interests.

Acknowledgements

Deleted: Finally, a recent study by Strommen et al. (2002) finds that inclusion of stochastic parameterizations amplifies the simulated atmospheric circulation response to sea surface temperature and Arctic sea ice anomalies. Such stochastic parameterizations may represent unresolved air-sea coupling processes in "coarse-resolution" climate models such as CESM2. Emerging efforts to develop mesoscale-eddy-resolving global coupled climate models may provide more definitive answers to this elusive challenge in the near future.*

789 We acknowledge the efforts of all those who contributed to producing the model simulations and
790 observational data sets used in this study. We thank L. Terray for providing the dynamical
791 adjustment results and K. McKinnon for providing the observational large ensemble results. We
792 sincerely appreciate the comments and suggestions from the Reviewers, which led to improved
793 clarity of presentation. The National Center for Atmospheric Research is sponsored by the
794 National Science Foundation.

795

796 **References**

- 797 Andrews, T., Bodas-Salcedo, A., Gregory, J. M., Dong, Y., Armour, K. C., Paynter, D., Lin, P.,
798 Modak, A., Mauritsen, T., Cole, J. N. S., Medeiros, B., Benedict, J. J., Douville, H.,
799 Roehrig, R., Koshiro, T., Kawai, H., Ogura, T., Dufresne, J. -L., Allan, R. P., and Liu, C.:
800 On the effect of historical SST patterns on radiative feedback, *J. Geophys. Res.-Atmos.*,
801 127, e2022JD036675, <https://doi.org/10.1029/2022JD036675>, 2022.
- 802 Barnes, E. A., Hurrell, J. W., and Uphoff, I. E.: Viewing forced climate patterns through an AI
803 lens, *Geophys. Res. Lett.*, 46, 13389–13398, <https://doi.org/10.1029/2019GL084944>, 2019.
- 804 Beusch, L., Gudmundsson, L., and Seneviratne, S. I.: Emulating Earth System Model
805 temperatures: from global mean temperature trajectories to grid-point level realizations on
806 land, *Earth Syst. Dyn. Discuss.*, <https://doi.org/10.5194/esd-2019-34>, 2019.
- 807 *Bódai, T., G. Drótos, M. Herein, F. Lunkeit, and V. Lucarini: The Forced Response of the*
808 *El Niño–Southern Oscillation–Indian Monsoon Teleconnection in Ensembles of Earth*
809 *System Models*, *J. Climate*, 33, 2163–2182, <https://doi.org/10.1175/JCLI-D-19-0341.1>,
810 2020.
- 811 *Bódai, T., J.-Y. Lee, and A. Sundaresan: Sources of Nonergodicity for Teleconnections as Cross-*
812 *Correlations*, *Geophys. Res. Lett.*, 49, 8, e2021GL096587, doi: 10.1029/2021GL096587,
813 2022.
- 814 Bonfils, C. J. W., Santer, B. D., Fyfe, J. C., Marvel, K., Phillips, T. J., and Zimmerman, S. R. H.:
815 Human influence on joint changes in temperature, rainfall and continental aridity. *Nat.*
816 *Clim. Change*, 10, 726–731, <https://doi.org/10.1038/s41558-020-0821-1>, 2020.
- 817 Branstator, G. and Teng, H.: Two limits of initial-value decadal predictability in a CGCM, *J.*
818 *Climate*, 23, 6292–6311, <https://doi.org/10.1175/2010JCLI3678.1>, 2010.

Formatted: Font: Italic

Formatted: Font: Italic

819 Capotondi, A., Deser, C., Phillips, A., Okumura, Y. and Larson, S.: ENSO and Pacific
820 Decadal Variability in the Community Earth System Model Version 2, *J. Adv. Model.*
821 *Earth Sy.*, 12, e2019MS002022, <https://doi.org/10.1029/2019MS002022>, 2020.

822 Compo, G. P., Whitaker, J. S., Sardeshmukh, P. D., Matsui, N., Allan, R. J., Yin, X., Gleason,
823 B.E., Vose, R.S., Rutledge, G., Bessemoulin, P., Brönnimann, S., Brunet, M., Crouthamel,
824 R.I., Grant, A.N., Groisman, P.Y., Jones, P.D., Kruk, M.C., Kruger, A.C., Marshall, G.J.,
825 Maugeri, M., Mok, H.Y., Nordli, Ø., Ross, T.F., Trigo, R.M., Wang, X.L., Woodruff, S.D.
826 and Worley, S.J.: The twentieth century reanalysis project, *Q. J. Roy. Meteor. Soc.*, 137, 1–
827 28, <https://doi.org/10.1002/qj.776>, 2011.

828 Davenport, F. V. and Diffenbaugh, N. S.: Using machine learning to analyze physical causes of
829 climate change: A case study of U.S. Midwest extreme precipitation, *Geophys. Res.*
830 *Lett.*, 48, e2021GL093787. <https://doi.org/10.1029/2021GL093787>, 2021.

831 Deser, C., Phillips, A., Bourdette, V., and Teng, H. Y.: Uncertainty in climate change
832 projections: The role of internal variability, *Clim. Dynam.*, 38, 527–546.
833 <https://doi.org/10.1007/s00382-010-0977-x>, 2012.

834 Deser, C., Phillips, A., Alexander, M. A., and Smoliak, B. V.: Projecting North American
835 climate over the next 50 years: Uncertainty due to internal variability. *J. Climate*, 27, 2271–
836 2296, <https://doi.org/10.1175/JCLI-D-13-00451.1>, 2014.

837 Deser, C., Terray, L., and Phillips, A. S.: Forced and internal components of winter air
838 temperature trends over North America during the past 50 years: Mechanisms and
839 implications, *J. Climate*, 29, 2237–2258. <https://doi.org/10.1175/JCLI-D-15-0304.1>, 2016.

840 Deser, C., Simpson, I. R., McKinnon K. A., and Phillips, A. S.: The Northern Hemisphere extra-
841 tropical atmospheric circulation response to ENSO: How well do we know it and how do

842 we evaluate models accordingly? J. Climate, 30, 5059-5082, [https://doi.org/10.1175/JCLI-](https://doi.org/10.1175/JCLI-D-16-0844.1)
843 [D-16-0844.1](https://doi.org/10.1175/JCLI-D-16-0844.1), 2017.

844 Deser, C., Hurrell, J. W., and Phillips, A.S.: The role of the North Atlantic Oscillation in
845 European Climate Projections, Clim. Dynam., 49, 3141–3157,
846 <https://doi.org/10.1007/s00382-016-3502-z>, 2017.

847 Deser, C., Simpson, I. R., Phillips, A. S., and McKinnon, K.A.: How well do we know ENSO's
848 climate impacts over North America, and how do we evaluate models accordingly? J.
849 Climate, 30, 4991-5014, <https://doi.org/10.1175/JCLI-D-17-0783.1>, 2018.

850 Deser, C.: Certain uncertainty: The role of internal climate variability in projections of regional
851 climate change and risk management. Earths Future, 8, e2020EF001854,
852 <https://doi.org/10.1029/2020EF001854>, 2020.

853 Deser, C., Lehner, F., Rodgers, K. B., Ault, T., Delworth, T. L., DiNezio, P. N., Fiore, A.,
854 Frankignoul, C., Fyfe, J. C., Horton, D. E., Kay, J. E., Knutti, R., Lovenduski, N. S.,
855 Marotzke, J., McKinnon, K. A., Minobe, S., Randerson, J., Screen, J. A., Simpson, I. R.,
856 and Ting, M.: Insights from earth system model initial-condition large ensembles and
857 future prospects. Nat. Clim. Change, 10, 277-286, [https://doi.org/10.1038/s41558-020-](https://doi.org/10.1038/s41558-020-0731-2)
858 [0731-2](https://doi.org/10.1038/s41558-020-0731-2), 2020^a.

859 Deser, C., Phillips, A. S., Simpson, I. R., Rosenbloom, N., Coleman, D., Lehner, F., Pendergrass,
860 A., DiNezio, P., and Stevenson, S.: Isolating the Evolving Contributions of Anthropogenic
861 Aerosols and Greenhouse Gases: A New CESM1 Large Ensemble Community Resource. J.
862 Climate, 33, 7835-7858, <https://doi.org/10.1175/JCLI-D-20-0123.1>, 2020^b.

863 Deser, C. and Phillips, A.S.: Defining the internal component of Atlantic Multidecadal
 864 Variability in a changing climate. *Geophys. Res. Lett.*, 48, e2021GL095023,
 865 <https://doi.org/10.1029/2021GL095023>, 2021.

866 DiNezio, P. N., Deser, C., Okumura, Y., and Karspeck, A.: Predictability of 2-year La Niña
 867 events in a coupled general circulation model, *Clim. Dyn.* 49, 4237–4261, 2017.

868 Dong, Y., Armour, K.C., Zelinka, M., Proistosescu, C., Battisti, D., Zhou, C., and Andrews, T.:
 869 Inter-model spread in the pattern effect and its contribution to climate sensitivity in CMIP5
 870 and CMIP6 models, *J. Climate*, <https://doi.org/10.1175/JCLI-D-19-1011.1>, 2020.

871 Eade, R., Smith, D., Scaife, A., Wallace, E., Dunstone, N., Hermanson, L., and Robinson, N.: Do
 872 seasonal-to-decadal climate predictions underestimate the predictability of the real
 873 world?, *Geophys. Res. Lett.*, 41, 5620– 5628, <https://doi.org/10.1002/2014GL061146>,
 874 2014.

875 [Fasullo, J. T. and R.S. Nerem: “Altimeter-era emergence of the patterns of forced sea-level rise](https://doi.org/10.1073/pnas.1813233115)
 876 [in climate models and implications for the future. *Proc. Natl Acad. Sci.*](https://doi.org/10.1073/pnas.1813233115)
 877 <https://doi.org/10.1073/pnas.1813233115>, 2018.

878 Fasullo, J., Phillips, A. S., and Deser, C.: Evaluation of leading modes of climate variability in
 879 the CMIP Archives, *J. Climate*, 33, 5527–5545, <https://doi.org/10.1175/JCLI-D-19-1024.1>,
 880 2020.

881 [Gettelman, A., Hannay, C., Bacmeister, J. T., Neale, R. B., Pendergrass, A. G., Danabasoglu, G.,](https://doi.org/10.1029/2019GL083978)
 882 [et al.: High climate sensitivity in the Community Earth System Model Version 2](https://doi.org/10.1029/2019GL083978)
 883 [\(CESM2\). *Geophys. Res. Lett.*, 46, 8329– 8337, https://doi.org/10.1029/2019GL083978,](https://doi.org/10.1029/2019GL083978)
 884 [2019.](https://doi.org/10.1029/2019GL083978)

Formatted: Font: Not Italic

Formatted: Font: Not Italic

Formatted: Font: Not Italic

Formatted: Font: Not Italic

Formatted: Hyperlink, Font: Times New Roman, Not Italic,
 Pattern: Clear

Field Code Changed

885 Gordon, E. M. and Barnes, E.A.: Incorporating uncertainty into a regression neural network
 886 enables identification of decadal state-dependent predictability, *Geophys. Res. Lett.*,
 887 e2022GL098635, <https://doi.org/10.1029/2022GL098635>, 2022.
 888 Gould, S. J.: *Wonderful Life: The burgess shale and the nature of history*, W. W. Norton & Co.,
 889 978-0-393-30700-9, 1989.
 890 Griffies, S. M. and Bryan, K.: Predictability of North Atlantic multidecadal climate
 891 variability, *Science*, 275, 181–184, <https://doi.org/10.1126/science.275.5297.181>, 1997.
 892 Guo, R. X., Deser, C., Terray, L., and Lehner, F.: Human influence on terrestrial precipitation
 893 trends revealed by dynamical adjustment, *Geophys. Res. Lett.*, 46, 3426-3434,
 894 <https://doi.org/10.1029/2018GL081316>, 2019.
 895 Hegerl, G.C., Zwiers, F. W. , Braconnot, P., Gillett, N. P., Luo, Y., Marengo Orsini, J. A.,
 896 Nicholls, N., Penner, J. E., and Stott, P. A.: Understanding and attributing climate change.
 897 In: *Climate Change 2007: The Physical Science Basis. Contribution of Working Group I to*
 898 *the Fourth Assessment Report of the Intergovernmental Panel on Climate Change*,
 899 Solomon, S., D. Qin, M. Manning, Z. Chen, M. Marquis, K.B. Averyt, M. Tignor and H.L.
 900 Miller (eds.), Cambridge University Press, Cambridge, United Kingdom and New York,
 901 NY, USA, 2007.
 902 Hurrell J. W., Kushnir, Y., Otttersen G., and Visbeck M. (eds): *The North Atlantic Oscillation:*
 903 *climate significance and environmental impact*, *Geophys. Monogr. Ser.*, 134, AGU,
 904 Washington, D. C., 2003.
 905 James, I. N. and James, P. M.: Spatial structure of ultra-low-frequency variability of the flow in a
 906 simple atmospheric circulation model. *Quart. J. Roy. Meteor. Soc.*, 118, 1211-1233,
 907 <https://doi.org/10.1002/qj.49711850810>, 1992.

908 Jin, E.K., Kinter, J.L., and Wang, B: Current status of ENSO prediction skill in coupled ocean–
 909 atmosphere models, *Clim. Dynam.* 31, 647–664, [https://doi.org/10.1007/s00382-008-0397-](https://doi.org/10.1007/s00382-008-0397-3)
 910 [3](https://doi.org/10.1007/s00382-008-0397-3), 2008.

911 Kay, J., Deser, C., Phillips, A., Mai, A., Hannay, C., Strand, G., Arblaster, J. M., Bates, S. C.,
 912 Danabasoglu, G., Edwards, J., Holland, M., Kushner, P., Lamarque, J. -F., Lawrence, D.,
 913 Lindsay, K., Middleton, A., Munoz, E., Neale, R., Oleson, K., Polvani, L. and Vertenstein,
 914 M.: The Community Earth System Model (CESM) Large Ensemble Project: A community
 915 resource for studying climate change in the presence of internal climate variability, *B. Am.*
 916 *Meteorol. Soc.*, 96, 1333–1349, <https://doi.org/10.1175/BAMS-D-13-00255.1>, 2015.

917 Klavans, J.M., Cane, M.A., Clement, A.C., and Murphy, L. N.: NAO predictability from external
 918 forcing in the late 20th century, *Npj Clim. Atmos. Sci.*, 4, 22 (2021),
 919 <https://doi.org/10.1038/s41612-021-00177-8>, 2021.

920 Lehner, F., Schurer, A. P., Hegerl, G. C., Deser, C., and Frölicher, T. L.: The importance of
 921 ENSO phase during volcanic eruptions for detection and attribution, *Geophys. Res. Lett.*
 922 43, 2851–2858, <https://doi.org/10.1002/2016GL067935>, 2016.

923 Lehner, F., Deser, C., and Terray, L.: Towards a new estimate of “time of emergence” of
 924 anthropogenic warming: insights from dynamical adjustment and a large initial-condition
 925 model ensemble. *J. Climate*, 30, 7739–7756, <http://doi.org/10.1175/JCLI-D-16-0792.1>,
 926 2017.

927 Lehner, F., Deser, C., Simpson, I. R., and Terray, L.: Attributing the US Southwest's recent shift
 928 into drier conditions, *Geophys. Res. Lett.*, 45, 6251–6261,
 929 <https://doi.org/10.1029/2018GL078312>, 2018.

930 Lehner, F., Deser, C., Maher, N., Marotzke, J., Fischer, E., Brunner, L., Knutti, R. and Hawkins,
 931 E.: Partitioning climate projection uncertainty with multiple large ensembles and
 932 CMIP5/6. *Earth Syst. Dynam. Discuss., Special Issue on Large Ensembles*, 11, 491–508,
 933 <https://doi.org/10.5194/esd-11-491-2020>, 2020.
 934 Leith, C. E.: The standard error of time-average estimates of climatic means, *J. Appl. Meteorol.*
 935 *Clim.*, 12(6), 1066–1069, [https://doi.org/10.1175/1520-](https://doi.org/10.1175/1520-0450(1973)012%3C1066:TSEOTA%3E2.0.CO;2)
 936 [0450\(1973\)012%3C1066:TSEOTA%3E2.0.CO;2](https://doi.org/10.1175/1520-0450(1973)012%3C1066:TSEOTA%3E2.0.CO;2), 1973.
 937 Lorenz, E. N.: Deterministic nonperiodic flow, *J. Atmos. Sci.*, 20, 130–141,
 938 [https://doi.org/10.1175/1520-0469\(1963\)020<0130:DNF>2.0.CO;2](https://doi.org/10.1175/1520-0469(1963)020<0130:DNF>2.0.CO;2), 1963.
 939 Madden, R. A.: Estimates of the natural variability of time-averaged sea-level pressure, *Mon.*
 940 *Weather. Rev.*, 104, 942–952, [https://doi.org/10.1175/1520-](https://doi.org/10.1175/1520-0493(1976)104%3C0942:EOTNVO%3E2.0.CO;2)
 941 [0493\(1976\)104%3C0942:EOTNVO%3E2.0.CO;2](https://doi.org/10.1175/1520-0493(1976)104%3C0942:EOTNVO%3E2.0.CO;2), 1975.
 942 Maher, N., Matei, D., Milinski, S., and Marotzke, J.: ENSO change in climate projections:
 943 Forced response or internal variability?, *Geophys. Res. Lett.*, 45, 11390–11398,
 944 <https://doi.org/10.1029/2018GL079764>, 2018.
 945 Maher, N., Milinski, S., Suarez-Gutierrez, L., Botzet, M., Dobrynin, M., Kornblueh, L., Kröger,
 946 J., Takano, Y., Ghosh, R., Hedemann, C., Li, C., Li, H., Manzini, E., Notz, D. Putrasahan,
 947 D., Boysen, L., Claussen, M., Ilyina, T., Olonscheck, D., Raddatz, T., Stevens, B., and
 948 Marotzke, J.: The Max Planck Institute Grand Ensemble: Enabling the exploration of
 949 climate system variability, *J. Adv. Model. Earth Sy.*, 11, 2050–2069,
 950 <https://doi.org/10.1029/2019MS001639>, 2019.

951 McGraw, M. C., Barnes, E. A., and Deser, C.: Reconciling the observed and modeled southern
 952 hemisphere circulation response to volcanic eruptions, *Geophys. Res. Lett.*, 43, 7259–7266,
 953 <https://doi.org/10.1002/2016GL069835>, 2016.

954 McKenna, C. M., and Maycock, A. C.: Sources of uncertainty in multimodel large ensemble
 955 projections of the winter North Atlantic Oscillation, *Geophys. Res. Lett.*, 48,
 956 e2021GL093258, <https://doi.org/10.1029/2021GL093258>, 2021.

957 McKinnon, K. A., A. Poppick, Dunn-Sigouin, E. and C. Deser: An ‘Observational Large
 958 Ensemble’ to compare observed and modeled temperature trend uncertainty due to internal
 959 variability. *J. Climate*, **90**, 7585-7598, doi:10.1175/JCLI-D-16-0905.1, 2017.

960 McKinnon, K. A and Deser, C.: Internal variability and regional climate trends in an
 961 Observational Large Ensemble, *J. Climate*, 31, 6783–6802, [https://doi.org/10.1175/JCLI-](https://doi.org/10.1175/JCLI-D-17-0901.1)
 962 [D-17-0901.1](https://doi.org/10.1175/JCLI-D-17-0901.1), 2018.

963 McKinnon, K. A. and Deser, C.: The inherent uncertainty of precipitation variability, trends, and
 964 extremes due to internal variability, with implications for Western US water resources, *J.*
 965 *Climate*, 34, 9605-9622, <https://doi.org/10.1175/JCLI-D-21-0251.1>, 2021.

966 Meehl, G., Hu, A. and Teng, H: Initialized decadal prediction for transition to positive phase of
 967 the Interdecadal Pacific Oscillation, *Nat. Commun.*, 7, 11718 (2016),
 968 <https://doi.org/10.1038/ncomms11718>, 2016.

969 Meehl, G.A., J.H. Richter, Teng, H., Capotondi, A., Cobb, K., Doblas-Reyes, F., Donat, M. G.,
 970 England, M. H., Fyfe, J. C., Han, W., Kim, H., Kirtman, B. P., Kushnir, Y., Lovenduski, N.
 971 S., Mann, M. E., Merryfield, W. J., Nieves, V., Pegion, K., Rosenbloom, N., Sanchez, S.
 972 C., Scaife, A. A., Smith, D., Subramanian, A. C., Sun, L., Thompson, D., Ummenhofer, C.
 973 C., and Xie, S. -P.: Initialized Earth system prediction from subseasonal to decadal

974 timescales, Nat. Rev. Earth Environ., 2, 340–357 (2021), [https://doi.org/10.1038/s43017-](https://doi.org/10.1038/s43017-021-00155-x)
 975 [021-00155-x](https://doi.org/10.1038/s43017-021-00155-x), 2021.
 976 Merrifield, A., Lehner, F., Xie, S. -P., and Deser, C.: Removing circulation effects to assess
 977 Central US land-atmosphere interactions in the CESM Large Ensemble, Geophys. Res.
 978 Lett., 44, 9938–9946, <https://doi.org/10.1002/2017GL074831>, 2017.
 979 Milinski, S., Maher, N., and Olonscheck, D.: How large does a large ensemble need to be?, Earth
 980 Syst. Dyn. Discuss., 11, 885–901, <https://doi.org/10.5194/esd-11-885-2020>, 2019.
 981 Newman, M.: Interannual to decadal predictability of tropical and North Pacific sea surface
 982 temperatures, J. Climate, 20, 2333–2356, <https://doi.org/10.1175/JCLI4165.1>, 2007.
 983 Newman, M., Alexander, M. A., Ault, T. R., Cobb, K. M., Deser, C., Di Lorenzo, E., Mantua, N.
 984 J., Miller, A. J., Minobe, S., Nakamura, H., Schneider, N., Vimont, D. J., Phillips, A. S.,
 985 Scott, J. D., and Smith, C. A.: The Pacific decadal oscillation, revisited, J. Climate, 29,
 986 4399–4427, <https://doi.org/10.1175/JCLI-D-15-0508.1>, 2016.
 987 O’Brien, J. P. and Deser, C.: Quantifying and understanding forced changes to unforced modes
 988 of atmospheric circulation variability over the North Pacific in a coupled model large
 989 ensemble, *J. Climate*, **36**, 17–35, doi: <https://doi.org/10.1175/JCLI-D-22-0101.1>, 2023.
 990 Olivarez, H. C., Lovenduski, N. S., Brady, R. X., Fay, A. R., Gehlen, M., Gregor, L.,
 991 Landschützer, P., McKinley, G. A., McKinnon, K. A., and Munro, D. R.: Alternate
 992 histories: Synthetic large ensembles of sea-air CO₂ flux, Global Biogeochem. Cy., 36,
 993 e2021GB007174, <https://doi.org/10.1029/2021GB007174>, 2022.
 994 Persad, G. G., and Caldeira, K.: Divergent global-scale temperature effects from identical
 995 aerosols emitted in different regions. Nat. Commun., 9, 3289,
 996 <https://doi.org/10.1038/s41467-018-05838-6>, 2018.

Deleted: 2

Formatted: Font: Italic

Formatted: Font: Not Bold

998 Rodgers, K. B., Lee, S. -S., Rosenbloom, N., Timmermann, A., Danabasoglu, G., Deser, C.,
 999 Edwards, J., Kim, J. -E., Simpson, I., Stein, K., Stuecker, M. F., Yamaguchi, R., Bodai, T.,
 1000 Chung, E. -S., Huang, L., Kim, W., Lamarque, J. -F., Lombardozzi, D., Wieder, W. R., and
 1001 Yeager, S. G.: Ubiquity of human-induced changes in climate variability. *Earth Sys.*
 1002 *Dyn.*, 12, 1393–1411, <https://doi.org/10.5194/esd-12-1393-2021>, 2021.
 1003 Rohde, R., Muller, R., Jacobsen, R., Perlmutter, S., Rosenfeld, A., Wurtele, J., Curry, J.,
 1004 Wickham, C., and Mosher, S.: Berkeley Earth temperature averaging process, *Geoinf.*
 1005 *Geostat. Overview*, 1:2, <https://doi.org/10.4172/2327-4581.1000103>, 2013.
 1006 Santer, B., Fyfe, J. C., Solomon, S., Painter, J. F., Bonfils, C., Pallotta, G., and Zelinka, M. D.:
 1007 Quantifying stochastic uncertainty in detection time of human-caused climate signals, *Proc.*
 1008 *Natl. Acad. Sci.*, 116, 19821–19827, <https://doi.org/10.1073/pnas.1904586116>, 2019.
 1009 Scaife, A. A., Arribas, A., Blockley, E., Brookshaw, A., Clark, R. T., Dunstone, N., Eade, R.,
 1010 Fereday, D., Folland, C. K., Gordon, M., Hermanson, L., Knight, J. R., Lea, D. J.,
 1011 MacLachlan, C., Maidens, A., Martin, M., Peterson, A. K., Smith, D., Vellinga, M.,
 1012 Wallace, E., Waters, J. and Williams, A.: Skillful long-range prediction of European and
 1013 North American winters, *Geophys. Res. Lett.*, 41, 2514–2519,
 1014 <https://doi.org/10.1002/2014GL059637>, 2014.
 1015 Scaife, A. A. and Smith, D.: A signal-to-noise paradox in climate science. *Npj Clim. Atmos.*
 1016 *Sci.*, 1, 28 (2018), <https://doi.org/10.1038/s41612-018-0038-4>, 2018.
 1017 Schneider, D. P., Deser, C., and Fan, T.: Comparing the impacts of tropical SST variability and
 1018 polar stratospheric ozone loss on the Southern Ocean westerly winds, *J. Climate*, 28, 9350-
 1019 9372, <https://doi.org/10.1175/JCLI-D-15-0090.1>, 2015.

1020 Schneider, U., Fuchs, T., Meyer-Christoffer, A., and Rudolf, B.: Global precipitation analysis
 1021 products of the GPCC. Global Precipitation Climatology Centre (GPCC), DWD, Internet
 1022 Publikation, 1-12.

1023 Shepherd, T.: Atmospheric circulation as a source of uncertainty in climate change
 1024 projections, *Nature Geosci.*, 7, 703–708 (2014), <https://doi.org/10.1038/ngeo2253>, 2014.

1025 Sippel, S. Meinshausen, N., Merrifield, A., Lehner, F., Pendergrass, A. G., Fischer, E., and
 1026 Knutti, R.: Uncovering the forced climate response from a single ensemble member using
 1027 statistical learning, *J. Climate*, 32, 5677–5699, <https://doi.org/10.1175/JCLI-D-18-0882.1>,
 1028 2019.

1029 Slingo, J., P. Bates, P. Bauer, S. Belcher, T. Palmer, G. Stephens, B. Stevens, T. Stocker, G.
 1030 Deutsch: Ambitious partnership needed for reliable climate prediction. *Nature Climate*
 1031 *Change*. doi:10.1038/s41558-022-01384-8, 2022.

1032 Smith, D., Eade, R., Scaife, A. A., Caron, L. -P., Danabasoglu, G., DelSole, T. M., Delworth, T.,
 1033 Doblas-Reyes, F. J., Dunstone, N. J., Hermanson, L., Kharin, V., Kimoto, M., Merryfield,
 1034 W. J., Mochizuki, T., Müller, W. A., Pohlmann, H., Yeager, S., and Yang, X: Robust skill
 1035 of decadal climate predictions, *Npj Clim. Atmos. Sci.*, 2, 13 (2019),
 1036 <https://doi.org/10.1038/s41612-019-0071-y>, 2019.

1037 Smith, D. M. et al. North Atlantic Climate far more predictable than models imply, *Nature*, 583,
 1038 796–800, 2020.

1039 Smith, D. M., Scaife, A. A., Eade, R., Athanasiadis, P., Bellucci, A., Bethke, I., Bilbao, R.,
 1040 Borchert, L. F., Caron, L.P., Counillon, F., Danabasoglu, G., Delworth, T., Doblas-Reyes,
 1041 F. J., Dunstone, N.J., Estella-Perez, V., Flavoni, S., Hermanson, L., Keenlyside, N., Kharin,
 1042 V., Kimoto, M., Merryfield, W. J., Mignot, J., Mochizuki, T., Modali, K., Monerie, P. A.,

Deleted: (2020)

Deleted:

1045 Müller, W. A., Nicolí, D., Ortega, P., Pankatz, K., Pohlmann, H., Robson, J., Ruggieri, P.,
 1046 Sospedra-Alfonso, R., Swingedouw, D., Wang, Y., Wild, S., Yeager, S., Yang, X., and
 1047 Zhang, L.: North Atlantic climate far more predictable than models imply, *Nature*, 583,
 1048 796–800, <https://doi.org/10.1038/s41586-020-2525-0>, 2020.

1049 Smoliak, B. V., Wallace, J. M., Lin, P., and Fu, Q.: Dynamical adjustment of the Northern
 1050 Hemisphere surface air temperature field: Methodology and application to observations, *J.*
 1051 *Climate*, 28, 1613–1629. <https://doi.org/10.1175/JCLI-D-14-00111.1>, 2015.

1052 Stevenson, S., Fox-Kemper, B., Jochum, M., Neale, R., Deser, C., and Meehl, G.: Will there be
 1053 a significant change to El Nino in the 21st Century?, *J. Climate*, 25, 2129–2145,
 1054 <https://doi.org/10.1175/JCLI-D-11-00252.1>, 2012.

1055 Suarez-Gutierrez, L., Milinski, S., and Maher, N.: Exploiting large ensembles for a better yet
 1056 simpler climate model evaluation, *Clim. Dynam.*, 57, 2557–2580 (2021),
 1057 <https://doi.org/10.1007/s00382-021-05821-w>, 2021.

1058 Swart, N. C., Fyfe, J. C., Hawkins, E., Kay, J. E., and Jahn A.: Influence of internal variability on
 1059 Arctic sea-ice trends. *Nat. Clim. Change*, 5, 86–89, <https://doi.org/10.1038/nclimate2483>,
 1060 2015.

1061 Tebaldi, C., Dorheim, K., Wehner, M., Leung, R.: Extreme metrics from large ensembles:
 1062 investigating the effects of ensemble size on their estimates, *Earth Syst. Dynam.*, 12 (4),
 1063 1427–1501, <https://doi.org/10.5194/esd-12-1427-2021>, 2021.

1064 Tél, T., Bódai, T., Drótos, G., Haszpra, T., Herein, M., Kaszás, B., and Vincze, M.: The theory
 1065 of parallel climate realizations, *J. Stat. Phys.*, 179, 1496–1530,
 1066 <https://doi.org/10.1007/s10955-019-02445-7>, 2020.

Deleted: Strommen, K., Juricke, S., and Cooper, F.: Improved teleconnection between Arctic sea ice and the North Atlantic Oscillation through stochastic process representation, *Weather Clim. Dynam.*, 3, 951–975, <https://doi.org/10.5194/wcd-3-951-2022>, 2022.

1072 Terray, L.: A dynamical adjustment perspective on extreme event attribution, *Weather Clim.*
 1073 *Dynam.*, 2, 971–989, <https://doi.org/10.5194/wcd-2-971-2021>, 2021.
 1074 Thompson, D. W. J., Barnes, E. A., Deser, C., Foust, W. E., and Phillips, A. S.: Quantifying the
 1075 role of internal climate variability in future climate trends, *J. Climate*, 28, 6443–6456,
 1076 <https://doi.org/10.1175/JCLI-D-14-00830.1>, 2015.
 1077 Trenary, L. and DelSole, T.: Does the Atlantic Multidecadal Oscillation Get Its Predictability
 1078 from the Atlantic Meridional Overturning Circulation?, *J. Climate*, 29, 5267–5280,
 1079 <https://doi.org/10.1175/JCLI-D-16-0030.1>, 2016.
 1080 Wallace, J.M., Deser, C., Smoliak, B. V., and Phillips, A. S.: Attribution of climate change in
 1081 the presence of internal variability, In *Climate Change: Multidecadal and Beyond* (Eds:
 1082 C.P. Chang, M. Ghil, M. Latif, and J. M. Wallace), *World Scientific Series on Asia-Pacific*
 1083 *Weather and Climate*, 6, 1–29, https://doi.org/10.1142/9789814579933_0001, 2013.
 1084 Wang, C., Deser, C., Yu, J. -Y., DiNezio, P., and Clement, A.: El Nino and Southern Oscillation
 1085 (ENSO): A Review. *Coral Reefs of the Eastern Pacific*, P. Glynn, D. Manzello and I.
 1086 Enochs, Eds., *Springer Science Publisher*, 4, 85–106, [https://doi.org/10.1007/978-94-017-](https://doi.org/10.1007/978-94-017-7499-4_4)
 1087 [7499-4_4](https://doi.org/10.1007/978-94-017-7499-4_4), 2017.
 1088 Wills, R. C. J., Battisti, D. S., Armour, K. C., Schneider, T., and Deser, C.: Pattern recognition
 1089 methods to separate forced responses from internal variability in climate model ensembles
 1090 and observations, *J. Climate*, 33, 8693–8719, <https://doi.org/10.1175/JCLI-D-19-0855.1>,
 1091 2020.
 1092 Wittenberg, A. T.: Are historical records sufficient to constrain ENSO simulations?, *Geophys.*
 1093 *Res. Lett.*, 36, L12702, <https://doi.org/10.1029/2009GL038710>, 2009.

1094 Wu, X., Okumura, Y. M., Deser, C., and DiNezio, P. N.: Two-year dynamical predictions of
 1095 ENSO event duration during 1954–2015, *J. Climate*, 34(10), 4069–4087,
 1096 <https://doi.org/10.1175/JCLI-D-20-0619.1>, 2021.

1097 Yeager, S. Danabasoglu, D., Rosenbloom, N. A., Strand, W., Bates, S. C., Meehl, G. A.,
 1098 Karspeck, A. R., Lindsay, K., Long, M. C., Teng, H., and Lovenduski, N. S.: Predicting
 1099 near-term changes in the Earth System: A large ensemble of initialized decadal prediction
 1100 simulations using the Community Earth System Model, *Bull. Am. Meteorol. Soc.* 99, 1867–
 1101 1886, <https://doi.org/10.1175/BAMS-D-17-0098.1>, 2018.

1102 Zhang, R., Sutton, R., Danabasoglu, G., Kwon, Y.-O., Marsh, R., Yeager, S. G., Amrhein, D. E.,
 1103 and Little, C. M.: A review of the role of the Atlantic Meridional Overturning Circulation
 1104 in Atlantic Multidecadal Variability and associated climate impacts, *Rev. Geophys.*, 57,
 1105 316–375, <https://doi.org/10.1029/2019RG000644>, 2019.

Formatted: Font: Italic

Formatted: Font: Italic

Deleted: 18